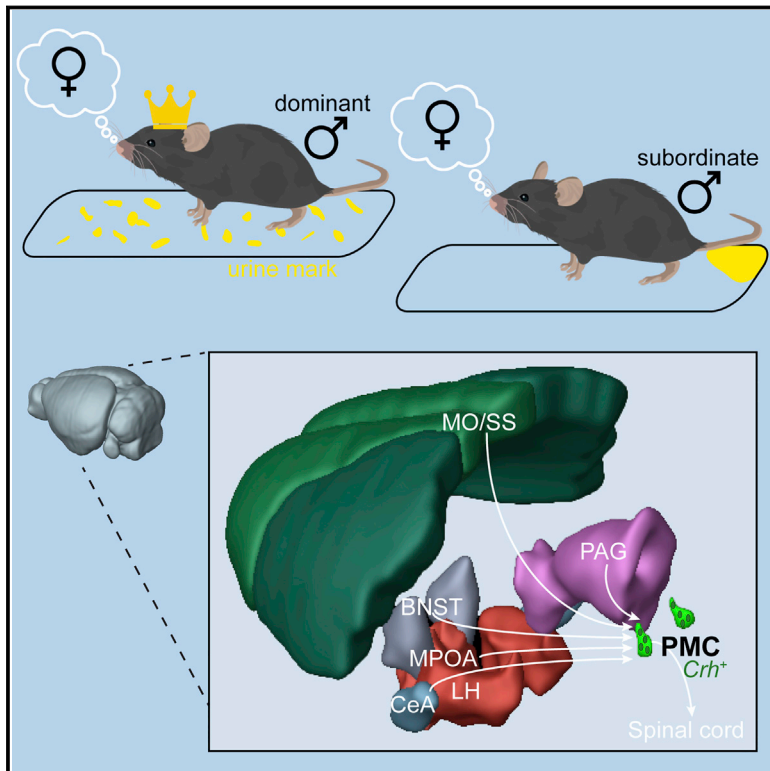


# Central Control Circuit for Context-Dependent Micturition

## Graphical Abstract



## Authors

Xun Helen Hou, Minsuk Hyun, Julian Taranda, ..., Mark Lawrence Zeidel, Pavel Osten, Bernardo Luis Sabatini

## Correspondence

bsabatini@hms.harvard.edu

## In Brief

How are olfactory and social cues integrated in the mouse brain to control where and under what circumstances mice urinate?

## Highlights

- Male lab mice regulate micturition behavior based on context and social rank
- PMC *Crh*<sup>+</sup> neurons comprise a command output of the brainstem controlling micturition
- Inputs from diverse brain regions converge onto *Crh*<sup>+</sup> PMC neurons
- One input, MPOA GABAergic neurons, modulates rank-dependent micturition patterns



# Central Control Circuit for Context-Dependent Micturition

Xun Helen Hou,<sup>1</sup> Minsuk Hyun,<sup>1</sup> Julian Taranda,<sup>2</sup> Kee Wui Huang,<sup>1</sup> Emmalee Todd,<sup>1</sup> Danielle Feng,<sup>1</sup> Emily Atwater,<sup>1</sup> Donyell Croney,<sup>1</sup> Mark Lawrence Zeidel,<sup>3</sup> Pavel Osten,<sup>2</sup> and Bernardo Luis Sabatini<sup>1,4,\*</sup>

<sup>1</sup>Howard Hughes Medical Institute, Department of Neurobiology, Harvard Medical School, Boston, MA 02115, USA

<sup>2</sup>Cold Spring Harbor Laboratory, Cold Spring Harbor, NY 11724, USA

<sup>3</sup>Beth Israel Deaconess Medical Center, Harvard Medical School, Boston, MA 02115, USA

<sup>4</sup>Lead Contact

\*Correspondence: [bsabatini@hms.harvard.edu](mailto:bsabatini@hms.harvard.edu)

<http://dx.doi.org/10.1016/j.cell.2016.08.073>

## SUMMARY

Urine release (micturition) serves an essential physiological function as well as a critical role in social communication in many animals. Here, we show a combined effect of olfaction and social hierarchy on micturition patterns in adult male mice, confirming the existence of a micturition control center that integrates pro- and anti-micturition cues. Furthermore, we demonstrate that a cluster of neurons expressing corticotropin-releasing hormone (*Crh*) in the pontine micturition center (PMC) is electrophysiologically distinct from their *Crh*-negative neighbors and sends glutamatergic projections to the spinal cord. The activity of PMC *Crh*-expressing neurons correlates with and is sufficient to drive bladder contraction, and when silenced impairs micturition behavior. These neurons receive convergent input from widespread higher brain areas that are capable of carrying diverse pro- and anti-micturition signals, and whose activity modulates hierarchy-dependent micturition. Taken together, our results indicate that PMC *Crh*-expressing neurons are likely the integration center for context-dependent micturition behavior.

## INTRODUCTION

The process of releasing urine, referred to as micturition, serves an essential physiological function to expel waste and maintain water balance. Micturition is also critical for social communication in many animal species; volatile and non-volatile components in urine convey information about the individual, including its sex, species, and identity (Bacchini et al., 1992; Beynon et al., 2002; Brennan and Keverne, 2004; Hurst and Beynon, 2004; Hurst et al., 1998; Kaur et al., 2014; Singer et al., 1997; Yamaguchi et al., 1981; Yamazaki et al., 1983). Consequently, in adult animals, the timing and location of micturition are tightly controlled and influenced by the sensory environment and past social experience (Ewer, 1968; Ralls, 1971). In male mice, olfactory cues that signal potential mates or competitors in the environment alter micturition patterns, with at least some of these

effects requiring intact vomeronasal sensing (Kaur et al., 2014; Leybold et al., 2002; Maruniak et al., 1986). Furthermore, following aggressive encounters that establish social hierarchy, a dominant male scatters urine throughout the cage, whereas the subordinate male, like females, limits micturition to restricted areas (Desjardins et al., 1973). Such behaviors suggest that micturition is under central neural control and that micturition control centers integrate complex information about sensory environment, experience, and internal state.

Classic studies identified a brainstem nucleus, the pontine micturition center (PMC; also known as Barrington's nucleus), as necessary for micturition. Bilateral lesion of the PMC prevents micturition in cats without affecting their drive to release urine (Barrington, 1925), a finding corroborated in humans with brainstem tumors and lesions (Betts et al., 1992). Furthermore, the PMC projects directly to spinal cord preganglionic bladder motor neurons, and polysynaptically to the bladder wall, as shown by anterograde tracing from the PMC in cats and retrograde tracing from the bladder wall in rats (Blok and Holstege, 1998; Sugaya et al., 1997). Lastly, the filling state of the bladder, as reflected in the activity of sensory afferents from the bladder, is thought to be relayed via the lumbosacral spinal cord to the PMC and periaqueductal gray (Blok and Holstege, 2000; Ding et al., 1997; Fowler et al., 2008; Rouzade-Dominguez et al., 2003; Takasaki et al., 2010).

The PMC has been hypothesized as the "command" center and a point of convergence of pro- and anti-micturition drives (Drake et al., 2010; de Groat and Wickens, 2013; Valentino et al., 1994). Nevertheless, electrical stimulation in the region of PMC in rats and cats can either trigger or inhibit bladder contraction (Holstege et al., 1986; Noto et al., 1989). Similarly, single-unit recordings in the PMC region in rats and cats reveal intermixed neurons that either increase or decrease firing during bladder contraction (de Groat et al., 1998; Mallory et al., 1991; Sasaki, 2004, 2005, Sugaya et al., 1997, 2003; Tanaka et al., 2003; Willette et al., 1988). These inconsistent results likely reflect the cellular heterogeneity of the PMC and the complex circuitry within the brainstem. Indeed, retrograde tracing from the lumbosacral spinal cord in rats identifies a subpopulation of PMC cells that express corticotropin-releasing hormone (*Crh*; also known as corticotropin-releasing factor [*Crfl*] as candidate spinal-projecting neurons (Keegan et al., 1994; Valentino et al., 1996, 2000; Vincent and Satoh, 1984). It is unknown if these neurons

are excitatory or inhibitory and if their activity is functionally pro- or anti-micturition. Thus, the cellular organization of the PMC, and how pro- and anti-micturition signals are conveyed to the PMC and relayed to the spinal cord, remain unclear.

Here, we establish that the activity of *Crh*-expressing (*Crh*<sup>+</sup>) neurons of the PMC correlates with bladder filling, is sufficient to trigger bladder contraction and emptying, and modulates normal micturition behavior. Electrophysiological and molecular characterization of *Crh*<sup>+</sup> PMC neurons reveals that they are distinct from their *Crh*-negative (*Crh*<sup>-</sup>) neighbors and that they are glutamatergic spinal-cord-projecting neurons. *Crh*<sup>+</sup> PMC neurons receive convergent input from multiple higher brain areas that are capable of carrying diverse pro- and anti-micturition signals. Reducing activity of GABAergic neurons in the medial preoptic area (MPOA), a candidate upstream area, alters micturition patterns and abolishes the differences in micturition between subordinate and dominant males. These results resolve controversies as to the function of *Crh*<sup>+</sup> neurons in micturition behavior and indicate that *Crh*<sup>+</sup> PMC neurons govern context-dependent micturition behaviors in mice.

## RESULTS

### Context and Social Hierarchy Dependent Micturition Behavior in Male Mice

Male mice modulate their micturition patterns depending on factors such as social rank (Desjardins et al., 1973) and olfactory cues (Kaur et al., 2014), indicating the existence of neural circuitry relaying higher-order brain function to bladder control. We examined if similar environmental and experiential control of urine release occurs in C57BL/6N mice in a laboratory setting. Pair-housed adult C57BL/6N male mice were separated into individual cages lined with filter paper with an olfactory stimulus (estrous female urine or saline) added to the cage center and rubbed onto the nose (Figure 1A). After 2 hr in the cage, mice were removed and tested for social hierarchy with their previous cage mate using the tube test (Lindzey et al., 1961), and the brains were processed for histology. In parallel, the distribution of urine spots on the paper was examined using fluorescence imaging.

Among the four categories (two-way combinations of dominant/subordinate and female urine/saline), only mice that are both dominant and exposed to female urine scatter a large number of urine spots throughout the arena (Figure 1A). In response to female urine, dominant mice deposit significantly more spots than their subordinate cage mates (dominant,  $119 \pm 19$  spots; subordinate,  $36 \pm 24$  spots; mean  $\pm$  SEM;  $n = 6$  mice each,  $p = 0.024$ ) (Figure 1B). This effect was not seen in response to saline (dominant,  $31 \pm 12$  spots; subordinate,  $23 \pm 6$  spots;  $n = 4$  mice each,  $p > 0.5$ ). In addition, dominant mice exposed to female urine deposit urine spots throughout the cage and preferentially toward the female urine whereas in the other contexts, mice deposit urine further from the stimulus center (average urine spot distance to stimulus center: dominant with female urine,  $8.1 \pm 0.5$  cm; subordinate with female urine,  $11.2 \pm 0.7$  cm; dominant with saline,  $11.6 \pm 0.4$  cm; subordinate with saline,  $12.1 \pm 0.8$  cm;  $p = 0.017$ , Kruskal-Wallis test) (Figure 1C). Furthermore, real-time tracking of

mouse position (Figures S1A and S1B) and micturition position (Figures S1C and S1D) in an open-field arena indicates that the average location of the urine spots is not predicted by the average location of the mouse.

These findings suggest the existence of a neural circuit in the mouse brain that integrates multiple factors, including social rank and sensory cues, to regulate micturition. A candidate region is the brainstem nucleus PMC. In order to determine if the activity of PMC correlates with degrees of marking behavior, we used the expression of the protein product of the immediate early gene *c-fos* as a readout of neural activation after marking (Figure 1D). The PMC was identified based on immunolabeling of the neighboring locus coeruleus (LC) for tyrosine hydroxylase (TH). The numbers of *c-fos*<sup>+</sup> cells in PMC and of urine spots deposited per animal positively correlate ( $n = 20$  mice,  $R^2 = 0.56$ ), suggesting a link between PMC activity and micturition behavior. The numbers of *c-fos*<sup>+</sup> cells are also higher in the LC of mice exposed to female urine (e.g., Figure 1D), but this was not analyzed further here.

### Neuronal Subpopulations within the PMC

The PMC contains neurons that express *Crh* and are labeled by retrograde tracers injected into the sacral spinal cord (Keegan et al., 1994; Valentino et al., 1996; Vincent and Satoh, 1984). We were able to visualize the PMC in coronal brainstem slices of transgenic mice produced by crossing *Crh*<sup>ires-Cre</sup> (Taniuchi et al., 2011) and Cre-dependent tdTomato reporter (*Rosa26*<sup>lsl-tdTomato</sup>) mice. In these slices, a collection of Cre-expressing (*Cre*<sup>+</sup>) cells marked by tdTomato is located medial to and juxtaposed with the LC, consistent with the described location of the PMC (Franklin and Paxinos, 2007) (Figure 2A). In situ hybridization confirmed *Cre* expression in PMC *Crh*<sup>+</sup> neurons in the *Crh*<sup>ires-Cre</sup> mice; 99% of *Crh*<sup>+</sup> cells express *Cre*, and 90% of *Cre*<sup>+</sup> cells express *Crh* ( $n = 179$  cells, 2 mice; Figure S2A). Furthermore, staining with general (DAPI) and neuron-specific (NeuN) nuclear markers revealed that each PMC contains a total of  $\sim 1,900$  cells and  $\sim 1,100$  neurons, with  $\sim 44\%$  of neurons being *Crh*<sup>+</sup> ( $n = 2$  mice, Figure 2B).

To determine if the *Crh*<sup>+</sup> neurons, the subset of PMC cells that can be uniquely identified and manipulated using the *Crh*<sup>ires-Cre</sup> transgenic mouse line, are functionally distinct from their *Crh*<sup>-</sup> neighbors, we characterized the intrinsic electrophysiological profiles of PMC neurons with whole-cell current-clamp recordings in acute coronal brainstem slices from postnatal day 17 (P17) to P21 *Crh*<sup>ires-Cre</sup>::*Rosa26*<sup>lsl-tdTomato</sup> mice (Figure S2C). Compared to *Crh*<sup>-</sup> neurons, *Crh*<sup>+</sup> neurons have lower  $R_m$  (*Crh*<sup>+</sup>:  $463 \pm 66$ ,  $n = 10$  cells; *Crh*<sup>-</sup>:  $734 \pm 80$  M $\Omega$ ,  $n = 8$  cells;  $p = 0.027$ ), higher  $C_m$  (*Crh*<sup>+</sup>:  $108 \pm 9$ ; *Crh*<sup>-</sup>:  $48 \pm 7$  pF;  $p = 0.0003$ ), lower induced firing rates (*Crh*<sup>+</sup>:  $7.8 \pm 1.1$ ; *Crh*<sup>-</sup>:  $26.4 \pm 4.7$  Hz with 100-pA current injection;  $p = 0.0015$ ), and lower voltage sag amplitude in response to  $-100$ -pA current injection (*Crh*<sup>+</sup>:  $1.8 \pm 1.3$ ; *Crh*<sup>-</sup>:  $8.0 \pm 2.3$  mV;  $p = 0.020$ ) (Figures S2D and S2E). Principal-component (PC) analysis of the electrophysiological parameters permitted good separation between *Crh*<sup>+</sup> and *Crh*<sup>-</sup> cells (Figure S2F; first PC explained 86% of the variance). Thus, PMC *Crh*<sup>+</sup> and *Crh*<sup>-</sup> neurons have distinct passive and active cellular properties, with further heterogeneity within each group.

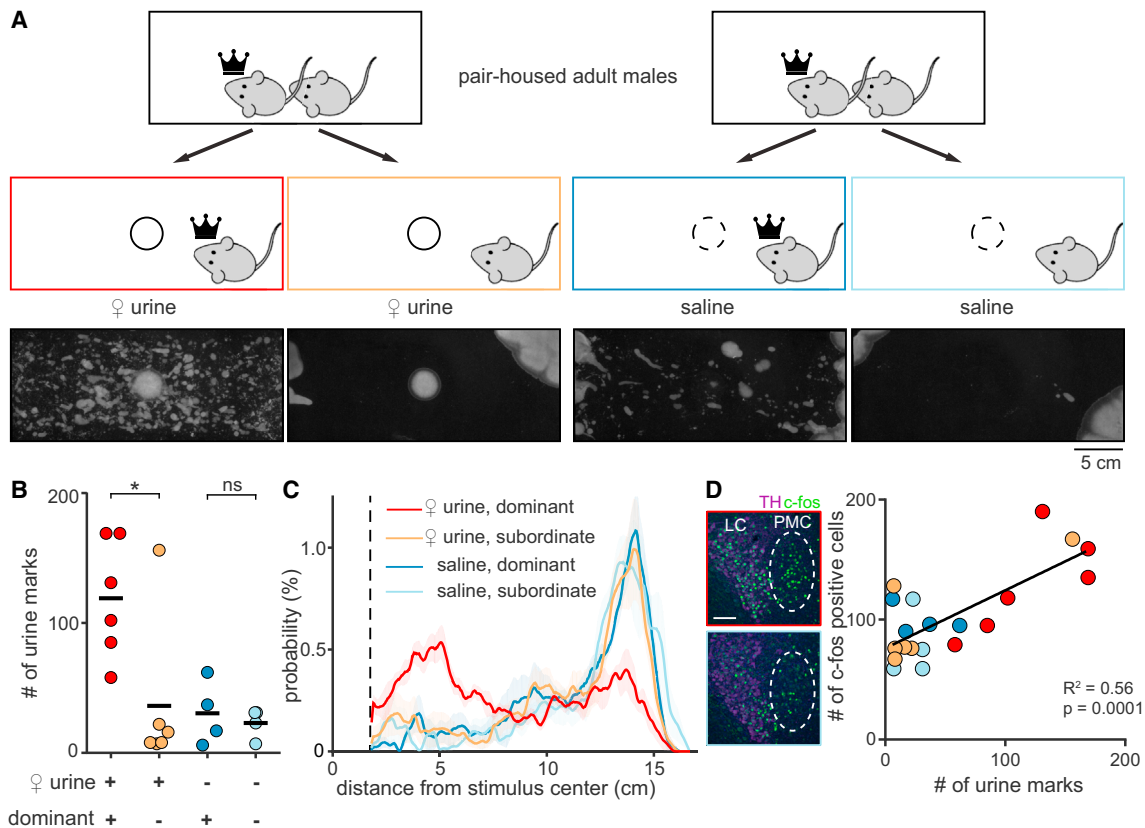


### Figure 1. Context-Dependent Territorial Marking Correlates with PMC Activity

(A) Schematic (top) of behavior setup and examples of urine marks deposited (bottom) demonstrating the context-dependency of territorial marking. Pair-housed adult males are separated and tested for 2 hr in response to olfactory stimuli: female urine or saline (solid or dotted circles). Social dominance (crown) is determined at the end of the 2-hr period.

(B) Quantification of urine marks deposited in each context. Black bars represent mean. \* $p < 0.05$ ; ns, not significant; two-tailed Mann-Whitney  $U$  test.

(C) Probability distribution of distances between urine-marked pixels and stimulus center for the four contexts with mean (solid lines) and SEM (shaded areas). The olfactory stimulus spot at cage center has a radius of 1.8 cm (dotted line).

(D) Example images (left) and quantification (right) of *c-fos* protein in the brainstem nucleus PMC in relation to micturition. Left: the PMC (dashed line) is identified by its location relative to locus coeruleus (LC), highlighted by immunostaining against tyrosine hydroxylase (TH; magenta). These are representative images from a dominant male in response to female urine (top, red border) and from a subordinate male in response to saline (bottom, blue border). Right: numbers of *c-fos*+ cells and urine marks positively correlate for each mouse (color scheme as in C). Scale bar, 100  $\mu$ m.

### *Crh*+ PMC Neurons are Glutamatergic and Project to the Sacral Spinal Cord

To determine if *Crh*+ neurons constitute a bladder-controlling output of the brainstem, we investigated the neurotransmitter identity and anatomy of these neurons. In situ hybridization was performed to detect mRNAs of *Crh*, vesicular glutamate transporters (Vglut; encoded by *Slc17a7*, *Slc17a6*, and *Slc17a8*), and glutamic acid decarboxylases (*Gad*; encoded by *Gad1* and *Gad2*) (Figure 2C). Single-cell mRNA counts of *Crh* correlated with those of Vglut and anti-correlated with those of *Gad* (Figure 2D). Nearly all *Crh*+ cells are glutamatergic (Vglut+ 94%,  $n = 444$  cells, 2 mice; Figure 2E), whereas the *Crh*- cells are a mix of glutamatergic (Vglut+ 53%) and GABAergic (GAD+ 45.2%). In situ hybridization using tissue from transgenic mice that express fluorophores in glutamatergic or GABAergic neurons yielded similar results (Figure S2B). The *Crh* mRNA count in each cell serves as a good classifier to differentiate between

glutamatergic and GABAergic cells in the PMC such that high *Crh* counts indicate that a cell is glutamatergic. Using receiver-operating characteristic (ROC) analysis, in which cells with *Crh* mRNA counts above a certain threshold are classified as glutamatergic, results in area under curve (AUC) of 0.84 (Figure 2D), closer to a perfect classifier (AUC = 1) than a “coin-toss” classifier (AUC = 0.5). Thus, *Crh* expression is strongly correlated with and predictive of expression of glutamatergic markers in the PMC.

To determine if *Crh*+ neurons of the PMC project to the spinal cord, we exploited human placental alkaline phosphatase (PLAP), a glycoposphatidylinositol anchored enzyme that robustly transports along neuronal processes and whose enzymatic activity is easily detected. A plasmid encoding a double-fluxed inverted open reading frame (DIO) of PLAP under transcriptional control of the CAG promoter (AAV-DIO-PLAP; Figure 2F) was generated to produce recombinant adeno-associated virus

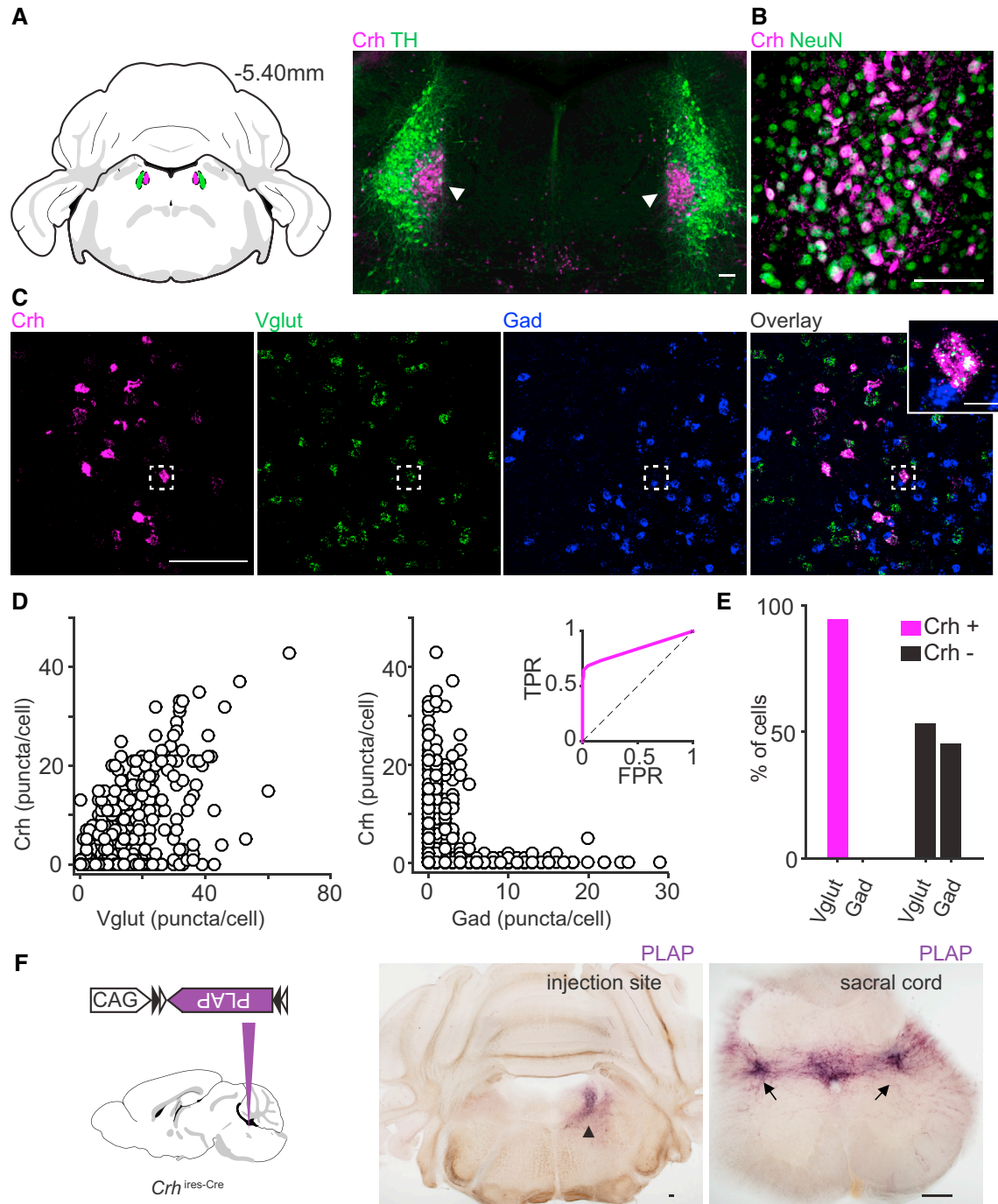


**Figure 2. *Crh*+ Neurons of the PMC Are Glutamatergic and Project to the Spinal Cord**

(A) Schematic (left) and fluorescently labeled coronal section (right) of the pons illustrating the location of the PMC next to the LC. The PMC (arrowheads) is identified by tdTomato fluorescence (magenta) from a *Crh<sup>ires-Cre</sup>::Rosa26<sup>sls</sup>-tdTomato* mouse, whereas immunostaining against TH (green) highlights the LC. Scale bar, 100  $\mu$ m.

(B) Higher-magnification image of the PMC from a section of a *Crh<sup>ires-Cre</sup>::Rosa26<sup>sls</sup>-tdTomato* mouse immunostained for NeuN (green). Scale bar, 100  $\mu$ m.

(C) In situ hybridization of *Crh* (magenta), *Vglut* (*Slc17a7*, *Slc17a6*, and *Slc17a8*, green), and *Gad* (*Gad1* and *Gad2*, red) mRNAs reveals that a vast majority of cells expressing *Crh* also express vesicular glutamate transporters, but not GABA synthetic enzymes. Scale bar, 100  $\mu$ m. The boxed region from the overlay is shown enlarged in inset (scale bar, 10  $\mu$ m).

(D) Quantification of detected mRNA copies per cell for *Crh* versus *Vglut* (left) and *Crh* versus *Gad* (right) showing a cell-by-cell correlation between the expression of *Crh* and *Vglut*, but not with that of *Gad*. Inset: ROC analysis shows that *Crh* copy number is a good classifier of *Vglut* versus *Gad* cell types (area under curve = 0.84). The true positive rate (TPR) versus false positive rate (FPR) of detecting a *Vglut* neuron based on a sliding threshold of *Crh* copy number is shown.

(legend continued on next page)

(AAV) that expresses PLAP in a Cre-dependent manner. AAV-DIO-PLAP injected unilaterally into the PMC of *Crh<sup>ires-Cre</sup>* mice yielded labeling of axon terminals bilaterally at the L6/S1 level in the spinal cord, the location of the sacral parasympathetic nucleus ( $n = 4$  mice) (Figure 2F). Thus, *Crh<sup>+</sup>* cells comprise half of the PMC neuronal population, are glutamatergic, and project to the sacral spinal cord.

### Activating PMC *Crh<sup>+</sup>* Neurons Triggers Bladder Contractions

The finding that glutamatergic *Crh<sup>+</sup>* neurons in PMC send long-range projections to spinal cord supports the hypothesis that *Crh<sup>+</sup>* PMC neurons are output neurons from the brain that control the bladder. If this is the case, then activating these neurons should be sufficient to evoke bladder contraction, and the activity of these neurons should correlate with intrinsic bladder activity. Furthermore, silencing these neurons should disrupt micturition behavior.

To address the first prediction, we investigated the effect of activating *Crh<sup>+</sup>* PMC neurons on bladder function. We expressed the light-activated cation channel channelrhodopsin-2 (ChR2) selectively in *Crh<sup>+</sup>* PMC neurons using Cre-dependent AAV (AAV-DIO-ChR2-tdTomato) and monitored bladder contractions using a catheter surgically inserted into the bladder (Figure 3A). Saline infusion into the bladder of an anesthetized mouse slowly fills the bladder at a constant rate, which triggers first non-micturating contractions followed by a micturating contraction. The latter is detected as a spike in bladder pressure followed by a fall in pressure to the lowest point, reflecting the now empty bladder (Uvin et al., 2012). Although the pressure spikes vary from mouse to mouse, the general pattern described above is preserved across mice. We recorded bladder pressure while light (473 nm, 15-ms pulses  $\times$  20 Hz for 5 s, delivered every 60 s) was delivered via an optic fiber implanted unilaterally above the PMC. In control mice expressing only tdTomato in *Crh<sup>+</sup>* PMC neurons (AAV-DIO-tdTomato), light delivery did not trigger bladder contraction (Figure 3A). In contrast, in mice expressing ChR2-tdTomato in PMC *Crh<sup>+</sup>* neurons, light delivery triggered time-locked bladder contraction in a majority of the trials, on top of the intrinsic bladder rhythm (Figure 3B). In separate trials, light was delivered at randomized intervals between 30 and 90 s to prevent possible entrainment of bladder contracture to the fixed 60-s interval used above. Light-triggered time-locked contractions were again seen in a majority of trials (Figure S3).

Alignment of bladder pressure recordings to the onset of light delivery revealed increases in pressure occurring during and outlasting light delivery in ChR2-expressing animals, but not in control tdTomato-expressing mice (Figure 3C). Bladder pressure was higher at the end of the 5-s light stimulus ( $P_{5\text{sec}}$ ) compared to before the stimulus ( $P_{\text{pre}}$ ), as seen across all trials in an example mouse (Figure 3D) and on average for five of six mice analyzed (ChR2:  $P_{5\text{sec}}/P_{\text{pre}} = 1.30 \pm 0.11$ ,  $n = 6$  mice; tdTomato control:

$0.96 \pm 0.02$ ,  $n = 4$  mice;  $p = 0.041$ ). Thus, activation of PMC neurons is sufficient to trigger time-locked bladder contraction.

### Activity of PMC *Crh<sup>+</sup>* Neurons Tracks Bladder Contraction and Micturition

To address the second prediction that the activity of *Crh<sup>+</sup>* PMC neurons is correlated to bladder contraction, we simultaneously monitored PMC activity and bladder pressure in anesthetized mice. Genetically encoded  $\text{Ca}^{2+}$  indicator GCaMP6s (Chen et al., 2013) was expressed in *Crh<sup>+</sup>* PMC neurons using Cre-dependent viruses (AAV-DIO-GCaMP6s). Fiber photometry (Cui et al., 2013; Gunaydin et al., 2014) was subsequently used to monitor activity-dependent  $\text{Ca}^{2+}$  entry in *Crh<sup>+</sup>* PMC neurons in vivo. A fiber optic was implanted in PMC and used to deliver 473-nm excitation light and collect fluorescence emission. Bladder contractions were measured with cystometry as described above (Figure 4A). As predicted, simultaneous recordings revealed that GCaMP6s fluorescence intensity, reflecting  $\text{Ca}^{2+}$  influx into *Crh<sup>+</sup>* PMC neurons, correlated with spike-like increases in bladder pressure, reflecting bladder contractions (Figure 4B). Aligning GCaMP6s fluorescence to the onset of bladder contraction (time = 0 defined as pressure reaching 5  $\text{cmH}_2\text{O}$  above baseline) showed that  $\text{Ca}^{2+}$  transients in PMC *Crh<sup>+</sup>* neurons were time-locked to bladder contraction (Figure 4C). Furthermore, cross-correlation of fluorescence and bladder pressure revealed a mean peak correlation coefficient higher than the shuffled data (data,  $0.62 \pm 0.07$ ; shuffled,  $-0.01 \pm 0.02$ ; mean  $\pm$  SEM,  $n = 4$  mice,  $p = 0.0286$ ) (Figure 4D).

To determine if micturition in freely moving mice coincides with activation of *Crh<sup>+</sup>* PMC neurons, we simultaneously monitored mouse locomotion, urine deposition, and  $\text{Ca}^{2+}$  entry into *Crh<sup>+</sup>* PMC neurons. Urine deposition was visualized by fluorescence with a blue excitation LED and a video camera (with GFP filter set) under the arena, whereas mouse position and posture were captured with an infrared (IR) LED and video camera above the arena (Figure 4E). To encourage micturition in this foreign and brightly lit arena, mice were treated with the diuretic furosemide. GCaMP6s fluorescence was collected with fiber photometry as described above while the mice moved freely, revealing that fluorescence increases at times of urine deposition (Figure 4F). On average and in individual micturition events, GCaMP6s fluorescence from *Crh<sup>+</sup>* PMC neurons rapidly increased before micturition, an effect absent in shuffled data (data, max  $\Delta F/F = 17.1\% \pm 1.6\%$ ; shuffled, max  $\Delta F/F = 3.6\% \pm 0.6\%$ ; mean  $\pm$  SEM; 75 micturition events,  $n = 4$  mice) (Figures 4G and 4H). Furthermore, two-color fiber photometry with the addition of a reference red channel in *Crh<sup>ires-Cre::Rosa26<sup>lsl-tdTomato</sup></sup>* animals injected with Cre-dependent GCaMP6s showed that intensity of GCaMP6s fluorescence, but not tdTomato, positively correlated with micturition (Figure S4), indicating that the correlated GCaMP6s signal could not be explained by movement artifacts. Thus, the bulk activity of *Crh<sup>+</sup>* PMC neurons correlates with bladder pressure

(E) Percentages of *Crh<sup>+</sup>* (magenta) and *Crh<sup>-</sup>* neurons (black) co-labeled by Vglut or Gad.

(F) Schematic of AAV-DIO-PLAP under the CAG promoter in a Cre-dependent manner (left). This virus, packaged as serotype 2.9, was injected into the PMC of *Crh<sup>ires-Cre</sup>* mice (middle, arrowhead), resulting in PLAP enzymatic activity (visualized by purple precipitate) in the PMC with axons found bilaterally in the spinal cord at the sacral parasympathetic nuclei (right, arrows). Scale bars, 100  $\mu\text{m}$ .

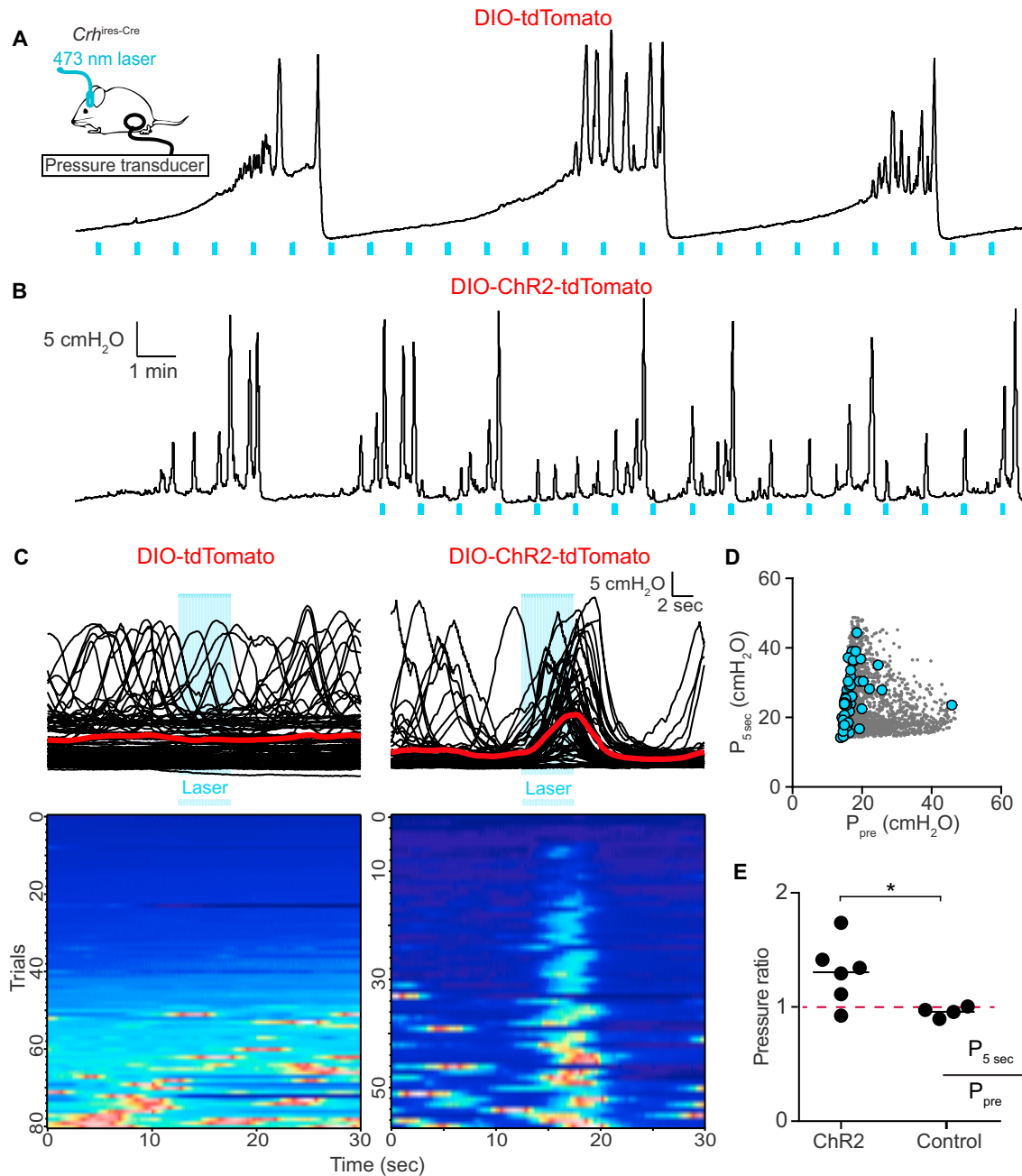


**Figure 3. Activation of *Crh*+ Neurons in the PMC Induces Bladder Contraction**

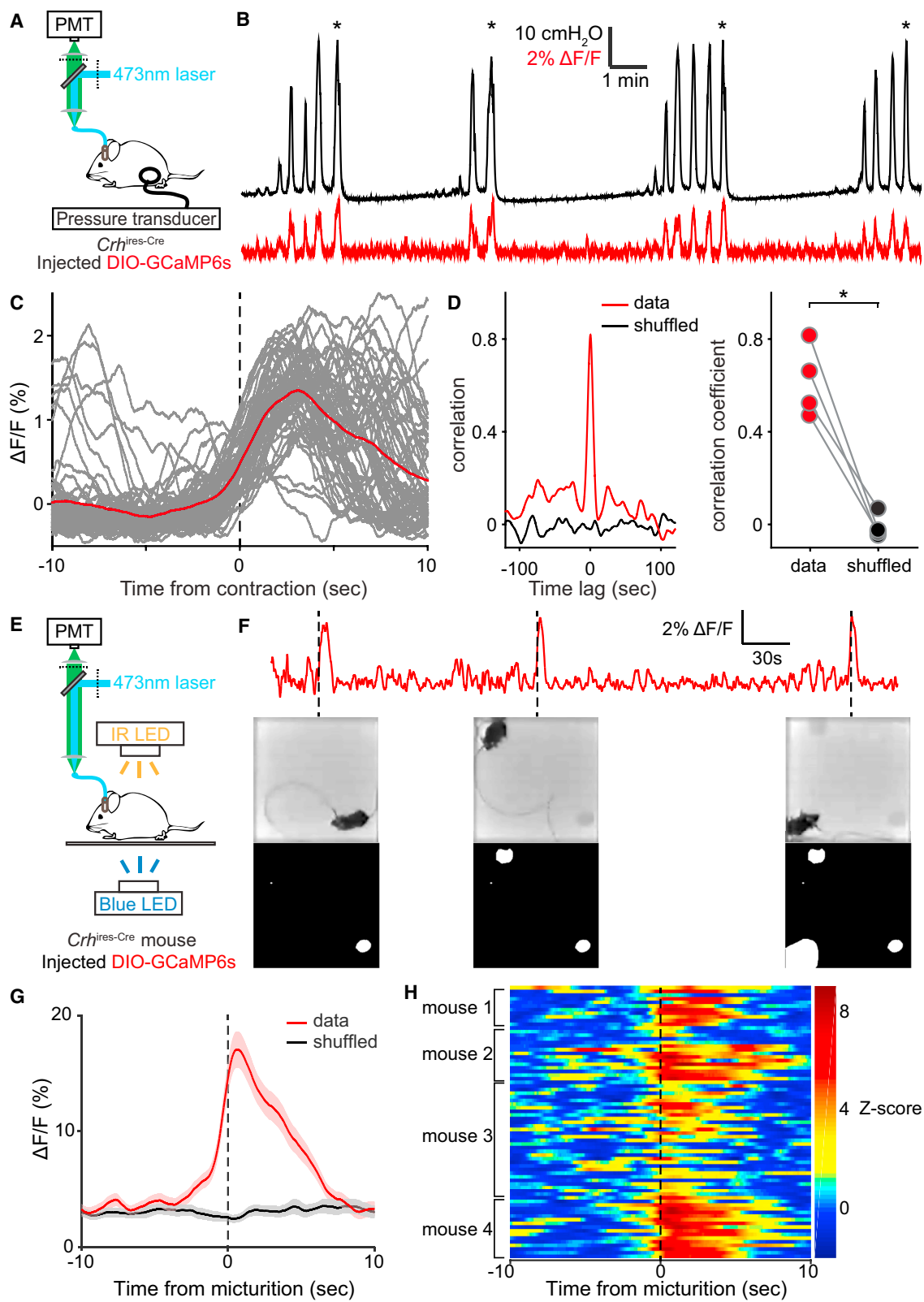
(A) Left: expression of ChR2-tdTomato or tdTomato alone (control) is induced virally in *Crh*+ neurons of PMC and a fiber optic is implanted to deliver 473 nm light to the PMC. Bladder pressure is monitored via an acutely implanted catheter. Right: example bladder pressure traces from a control mouse expressing tdTomato in PMC *Crh*+ neurons during delivery of light pulses (blue bars indicate 20 Hz stimulation with 15-ms light pulses for 5 s, repeated every minute).

(B) Example bladder pressure traces from a mouse expressing ChR2-tdTomato in PMC *Crh*+ neurons with the same light stimulation protocol.

(C) Top: overlay of 30 s of bladder pressure traces surrounding light delivery (blue bar, repeated every min). Bottom: same traces as in top panel shown in a heatmap (with warmer color indicating higher bladder pressure) sorted based on the amplitude prior to light delivery.

(D) Bladder pressure of mouse shown in (C) at laser onset and 5 s later (end of laser pulses, blue circles) compared to randomly chosen time points in the same recording (gray dots).

(E) Pressure ratios (defined as the ratio of bladder pressure at the end of laser pulses over the pressure at laser onset, averaged across trials for each mouse) are higher in AAV-DIO-ChR2-tdTomato-injected mice compared to AAV-DIO-tdTomato-injected mice. \* $p < 0.05$ , unpaired t test.



(legend on next page)

under anesthesia and is synchronized with initiation of micturition in freely moving mice.

### Reducing Activity of *Crh*+ PMC Neurons Impairs Micturition Behavior

To test the requirement of activity in *Crh*+ PMC neurons for micturition, we used the chemogenetic tool hM4Di, an engineered G<sub>i</sub> protein-coupled receptor activated by the inert ligand clozapine-N-oxide (CNO), to reduce the activity of *Crh*+ PMC neurons while adult male mice were exposed to female urine as in Figure 1 (AAV-hM4Di-mCherry, Figure 5A). Analysis of consecutive trials with intraperitoneal (i.p.) injection of either CNO (two trials) or saline (two trials) in randomized order demonstrated disrupted micturition in CNO trials (Figure 5B). Both the number of urine marks and the total area marked on filter paper, indicative of the total micturition volume, significantly decreased in CNO trials compared to saline trials (number of marks,  $p = 0.0024$ ; total area marked,  $p = 0.027$ ;  $n = 12$ ; Figure 5C). In contrast, CNO injection did not affect micturition in wild-type mice (number of marks:  $p = 0.38$ ; total area marked:  $p = 0.38$ ;  $n = 12$ ; Figure S5B). Furthermore, despite the decrease in total urine output in CNO-treated *Crh*<sup>ires-Cre</sup> mice, the spatial distribution of the remaining urine marks, as indicated by their average distance to stimulus center, was unaffected ( $p = 0.37$ ;  $n = 11$  mice; one mouse with zero urine marks in CNO was excluded from the analysis of urine mark distribution; Figure S5B). These results demonstrate that activation of hM4Di in *Crh*+ PMC neurons reduces the amount but not the pattern of urine release in freely moving mice, consistent with the hypothesis that activity of these cells normally drives micturition in the marking assay.

### *Crh*+ PMC Neurons Receive Converging Inputs from the Brain

The results presented above indicate that *Crh*+ neurons are descending command neurons that control bladder function. Thus, they are poised, anatomically and functionally, to integrate pro-micturition and anti-micturition inputs from relevant brain areas and transduce these changes into urine output. To identify candidate neurons throughout the brain that synapse onto *Crh*+ PMC neurons, we used rabies-based retrograde transsynaptic labeling (Wall et al., 2010; Wickersham et al., 2007). The number and distribution of candidate neurons presynaptic to *Crh*+ PMC neurons were determined with an unbiased and automated method that uses serial two-photon tomography (STP)

and 3D reconstruction to quantitatively map rabies-labeled neurons (Ragan et al., 2012) (Figure 6A).

As control experiments for the specificity of rabies infection to *Crh*+ neurons and candidate inputs, injection of glycoprotein-deleted, EGFP-encoding rabies virus pseudotyped with EnvA (RbV-EGFP) in *Crh*<sup>ires-Cre</sup> mice without helper viruses (AAV-DIO-TVA-mCherry and AAV-DIO-RG) showed no rabies infection in the injection site (Figure S6A), whereas omitting AAV-DIO-RG resulted in robust starter cell labeling in the PMC but no EGFP+ neurons elsewhere in the brain (Figure S6B). PMC and nearby areas were separately examined for the specificity of the starter cells (Figure 6B). Furthermore, as a control experiment to differentiate inputs to PMC from those to medial vestibular nucleus (MV), a nucleus containing *Crh*+ neurons posterior to the PMC and hence a potential source of starter cell contamination, *Crh*+ MV neurons were specifically targeted as starter cells. This experiment, using both helper viruses AAV-DIO-TVA-mCherry and AAV-DIO-RG as well as RbV-EGFP, revealed no significant overlap between the EGFP-labeled candidate inputs to MV (Figure S6C) and those to PMC described below.

Among 14 mice with robust and specific RbV starter cell labeling, 11 brains (6 males and 5 females) were sliced and examined for RbV labeled areas, and 3 brains (2 males and 1 female) were processed for whole-brain STP cell counting. In all 14 mice, dense candidate input cells to PMC *Crh*+ cells were observed in prefrontal areas, including anterior cingulate cortex (ACA) and prelimbic cortex (PL), as well as motor cortex (MO) and somatosensory cortex (SS). More posterior labeled areas included the bed nucleus of the stria terminalis (BST), including both anterior and posterior divisions (BSTa and BSTp), the MPOA, the paraventricular hypothalamic nucleus (PVH), the lateral hypothalamus (LHA), the posterior hypothalamus (PH), and the zona incerta (ZI). Central amygdalar nucleus (CEA) also contained dense labeling, as did midbrain regions, including periaqueductal gray (PAG), superior colliculus motor related (SCm), and midbrain reticular nucleus (MRN) (Figure 6C). These areas are a subset of the 27 brain regions identified with whole-brain STP cell counting that each contain at least 0.1% of total EGFP+ cells within each mouse (Table S1). Although the numbers of EGFP+ cells throughout the brain varied across mice (3,731–39,355 cells;  $n = 3$  mice), the fractions of cells labeled per region within each macro structure (cortex, cerebral nuclei, hypothalamus, and midbrain) were strikingly consistent (Figure 6D).

### Figure 4. Ca<sup>2+</sup> Influx into PMC *Crh*+ Neurons Is Correlated with Bladder Contraction and Micturition

- (A) Expression of GCaMP6s is induced virally in *Crh*+ neurons of PMC and a fiber optic coupled to a photomultiplier tube (PMT) is implanted to record fluorescence arising from Ca<sup>2+</sup> influx into PMC *Crh*+ neurons. Bladder pressure is monitored via an acutely implanted catheter.
- (B) Example bladder pressure (top, black) and time-locked fluorescence (bottom, red) traces. Micturition events are denoted with an asterisk (\*).
- (C) Overlay of 20 s segments of bladder pressure traces surrounding onset of bladder contraction (time = 0 s) with the averaged transient in red.
- (D) Left: cross-correlation between bladder pressure and fluorescence transients from the mouse as shown in (B) and (C) (red) compared to shuffled data. Right: summary of cross-correlation coefficients. \* $p < 0.05$ , two-tailed Mann-Whitney *U* test.
- (E) Behavioral arena for real-time tracking of mouse position, micturition, and fiber photometry in awake behaving male *Crh*<sup>ires-Cre</sup> mice injected with AAV-DIO-GCaMP6s.
- (F) Top: example fiber photometry trace from a male mouse expressing GCaMP6s in PMC *Crh*+ neurons, overlaid with black dotted bars indicating initiation of three micturition bouts. Middle: corresponding frames from mouse (middle) and urine (bottom) tracking videos at micturition initiation.
- (G) Averaged fiber photometry signals aligned to the initiation of each micturition event at  $t = 0$  ( $n = 4$  mice, 75 micturition events, red) or to shuffled micturition events (black). Shaded area represents SEM.
- (H) Heatmap of individual events from (C) aligned to micturition, with warmer color indicating higher Z score of  $\Delta F/F$  photometry values.

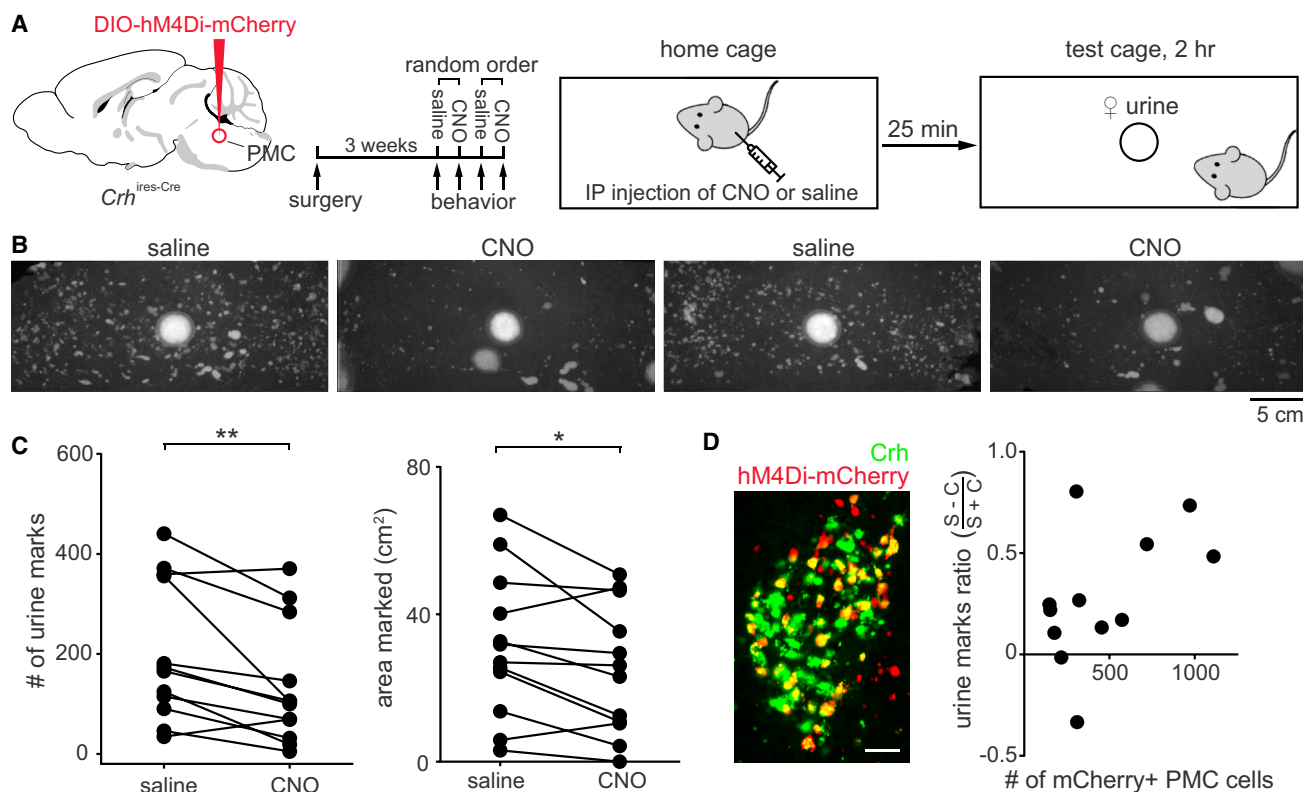


**Figure 5. Silencing *Crh*+ PMC Neurons Impairs Micturition and Urine Marking Behavior**

(A) Expression of hM4Di-mCherry is induced virally in *Crh*+ neurons of PMC. After 3 weeks of recovery and viral expression (the last week of which mice are habituated to unrestrained mock i.p. injection), each mouse was randomly assigned to receive CNO or saline i.p. injection and then returned to its home cage. 25 min after injection, mice were transferred to a test cage and the micturition patterns were imaged after 2 hr, as in Figure 1. In the subsequent session, animals were tested again, switching delivery of CNO or saline. The testing was repeated again, with each animal exposed once more to CNO and once more to saline on different days.

(B) Example micturition pattern from a single mouse with two trials each of CNO and saline i.p. injection.

(C) Number of urine marks deposited (left) and total area on the filter paper marked by urine (right) were both reduced in CNO trials compared to saline trials. \* $p < 0.05$ , \*\* $p < 0.01$ , Wilcoxon matched-pairs signed rank test.

(D) Example image (left) and quantification (right) of hM4Di-mCherry expression in relation to changes in micturition behavior. Left: representative image of hM4Di-mCherry expression in *Crh*+ PMC neurons (green, *Crh*<sup>ires-Cre</sup>::*Rosa26*<sup>sl-zsGreen</sup> mouse); right: urine marks ratio, defined as the difference in number of urine marks in saline (S) and CNO (C) conditions divided by their sum ( $S - C$ )/( $S + C$ ), positively correlates with the number of bilateral *Crh*+ PMC cells expressing hM4Di-mCherry. Scale bar, 50  $\mu$ m.

### Inhibiting MPOA GABAergic Neurons Modifies Micturition Patterns and Prevents Rank-Dependent Differences

A robust putative input to *Crh*+ PMC neurons implicated by rabies tracing experiments is the MPOA, a heterogeneous structure connected to multiple regions involved in social behaviors (Simerly and Swanson, 1986, 1988; Simerly et al., 1986). In situ hybridization revealed that the rabies-labeled neurons in the MPOA are largely *Gad*+ (including both *Gad1* and *Gad2*; 89.9%,  $n = 198$  cells/3 mice; Figures S7A and S7B), suggesting that MPOA mainly sends GABAergic input to *Crh*+ PMC neurons. To test the hypothesis that GABAergic MPOA neurons regulate micturition in a marking context, we inhibited bilateral MPOA neurons expressing the vesicular GABA transporter (*Vgat*; encoded by *Slc32a1*) by injecting AAV-DIO-hM4Di-mCherry into the MPOA of *Slc32a1*<sup>ires-Cre</sup> males and tested their micturition pattern in response to female urine (Figure 7A). With

CNO injection, the size of urine marks increased for both dominant and subordinate males (Figure 7B). Inhibiting MPOA *Vgat*+ neurons significantly decreased the number of urine marks while increasing the average size of each mark, leaving the total area marked unchanged (number of marks:  $p = 0.011$ ; total area marked:  $p = 0.64$ ; average mark size:  $p = 0.0012$ ;  $n = 13$  mice, Figures 7C and S7C). Furthermore, inhibiting *Vgat*+ MPOA neurons negates the differences in micturition behavior between dominant and subordinate males that were present in saline trials (number of marks: saline,  $p = 0.0012$ ; CNO,  $p = 0.38$ ; average mark size: saline,  $p = 0.0082$ ; CNO,  $p > 0.99$ .  $n = 13$  mice; Figure 7D). These results are consistent with a model in which silencing inhibitory MPOA inputs disinhibits *Crh*+ PMC neurons and that GABAergic MPOA neurons normally modulate micturition in the marking assay. Thus, these neurons influence both social-rank-dependent micturition patterns and the amount of urine released per bladder contraction.

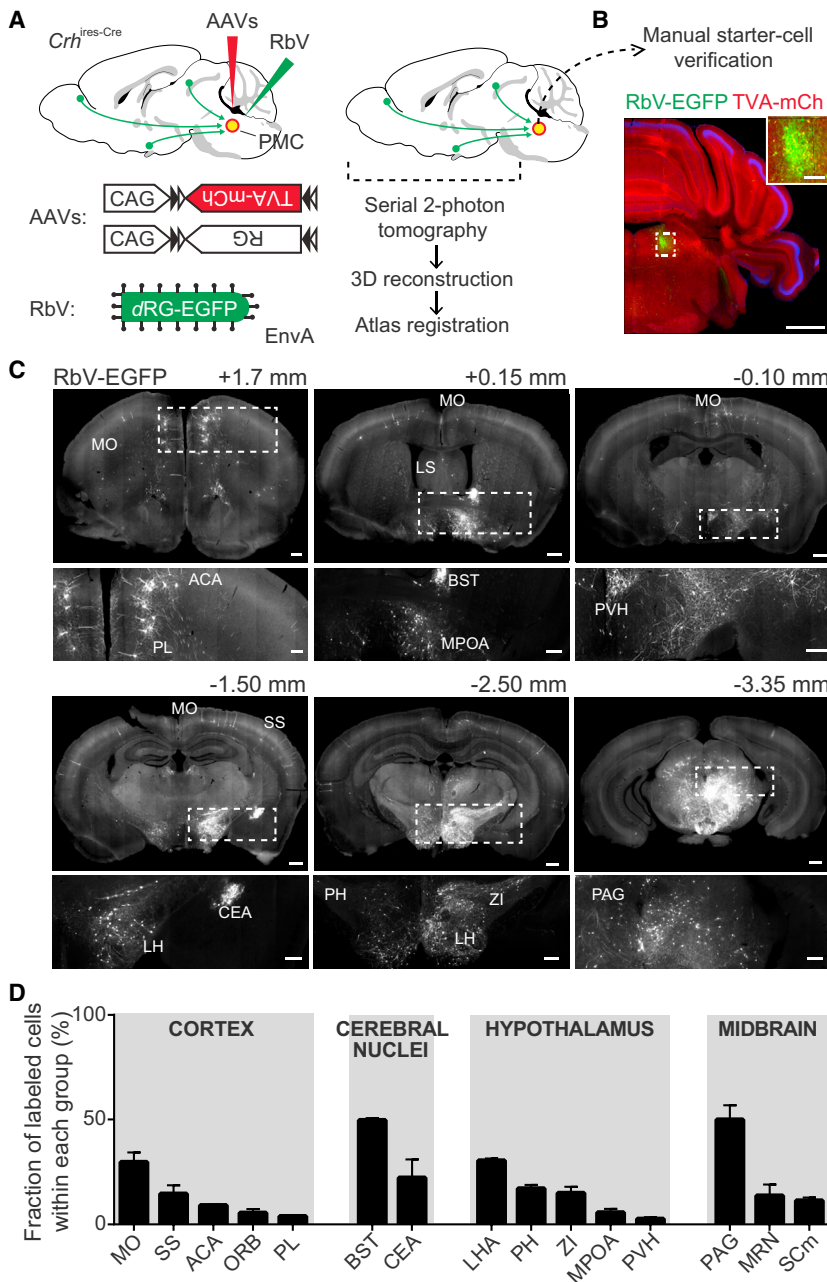


**Figure 6. *Crh*<sup>+</sup> PMC Neurons Receive Converging Inputs from Multiple Brain Regions**

(A) Schematic of rabies-based monosynaptic retrograde transsynaptic tracing from *Crh*<sup>+</sup> PMC neurons. The PMC of *Crh*<sup>ires-Cre</sup> mice was transduced unilaterally with two Cre-dependent AAVs encoding TVA-mCherry fusion protein (TVA-mCh) and rabies virus glycoprotein (RG), followed 3 weeks later by EnvA-pseudotyped, glycoprotein-deleted ( $\Delta$ RG) EGFP expressing rabies virus (RbV). After the rabies injection, the front part of the brains were embedded in agarose, imaged with a serial two-photon tomography (STP) system, reconstructed in 3D, and registered to a reference atlas for analysis.

(B) Brainstem sections containing the PMC were manually sliced and examined to identify starter cells in the injection site and to detect potential viral leak into nearby areas. Example starter cells in the PMC infected with both AAVs and RbV (yellow, enlarged in the inset). Scale bar represents 1 mm (125  $\mu$ m in the inset).

(C) Representative coronal sections of RbV-labeled cells displayed from anterior to posterior. RbV-EGFP-expressing cells reveal candidate areas projecting directly to *Crh*<sup>+</sup> neurons in the PMC. Approximate distances from the bregma are shown above the top panels. Regions inside the white dotted boxes are magnified and displayed in the bottom panels. MO, motor cortex; ORB, orbito-frontal cortex; ACA, anterior cingulate cortex; PL, prelimbic cortex; LS, lateral septum; SS, somato-sensory cortex; BST, bed nuclei of stria terminalis; MPOA, medial preoptic areas; PVH, paraventricular hypothalamic nucleus; LHA, lateral hypothalamus; ZI, zona incerta; CEA, central amygdalar nucleus; PH, posterior hypothalamus; PAG, periaqueductal gray; SCm, superior colliculus (motor related); MRN, midbrain reticular nucleus. Scale bar represents 500  $\mu$ m (top) and 250  $\mu$ m (bottom). The images in the top row are shown on the same grayscale. The contrast of each image in the bottom row has been adjusted to highlight cell bodies.

(D) The distribution of candidate neurons presynaptic to *Crh*<sup>+</sup> PMC neurons, shown as percentage of the total labeled cells with each group (cortex, cerebral nuclei, hypothalamus, and midbrain). Data represent mean  $\pm$  SEM.

## DISCUSSION

Animals integrate information from their environment, internal state, and experience to guide motor output and determine behavioral choices. In many mammals, including humans, micturition is one such behavioral choice. The release of urine reflects an ethologically relevant motor action undertaken in response to internal and external sensory inputs and is shaped by experience and context. We demonstrated that C57BL/6N male mice regulate micturition such that olfactory cues, combined with social rank, determine the pattern of urine deposition in a laboratory arena. Furthermore, we gained genetic control

over urine output, demonstrating that the activity of a subgroup of *Crh*<sup>+</sup> PMC is sufficient to trigger bladder contraction and normally promotes micturition. These pro-micturition neurons are sacral-cord-projecting glutamatergic neurons and receive convergent input from many upstream brain areas. Thus, *Crh*<sup>+</sup> neurons in the PMC comprise a command output of the brainstem that controls urine release and, due to convergent inputs from diverse brain regions, are poised to act as the integrating center that determines context-dependent urine release. Other brainstem neurons, possibly including the *Crh*<sup>-</sup> glutamatergic PMC neurons, may also project to the sacral cord and contribute to micturition behavior.

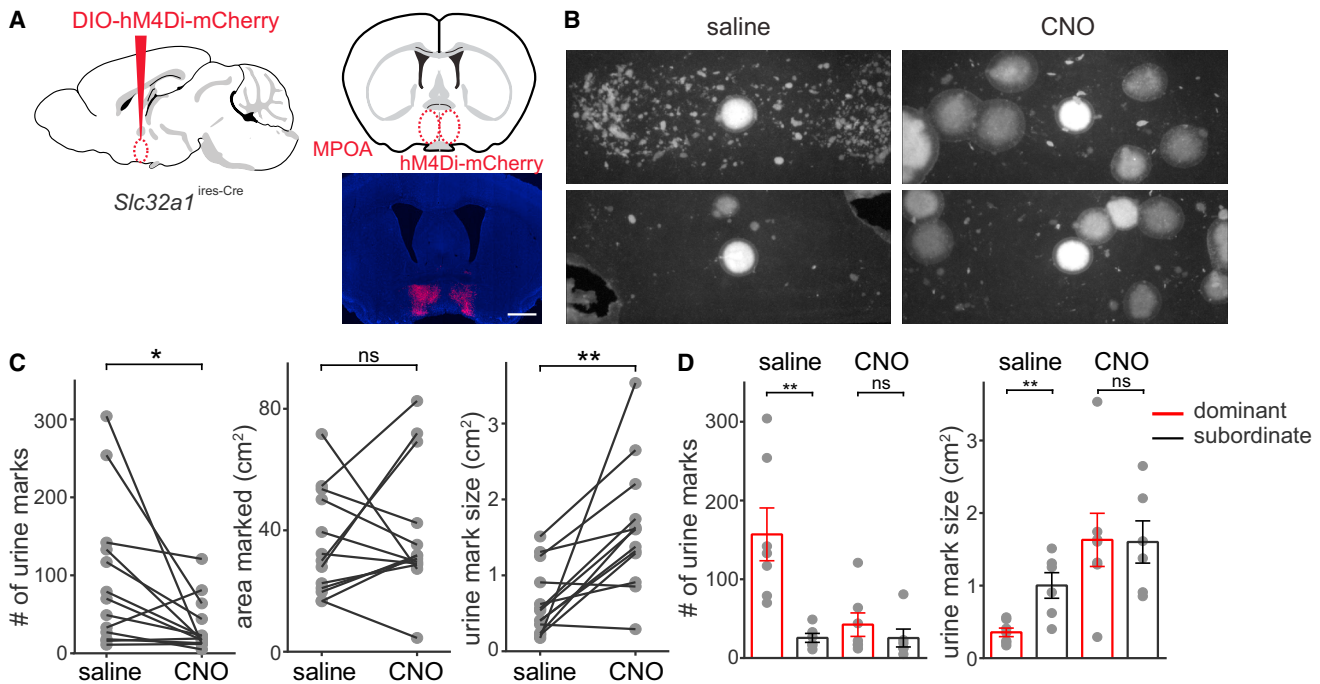


**Figure 7. GABAergic MPOA Neurons Modulate Rank-Dependent Micturition Patterns**

(A) Left: expression of hM4Di-mCherry is induced virally in MPOA GABAergic cells (defined by expression of vesicular GABA transporter [Vgat], encoded by *Slc32a1*); right: representative expression pattern of hM4Di-mCherry in MPOA. Scale bar, 1 mm.

(B) Example of urine marks deposited by a pair of co-housed adult males (top, dominant; bottom, subordinate) demonstrates modified micturition pattern in CNO trials (right) compared to saline trials (left).

(C) Summary data show that in CNO trials the number of urine marks deposited decreases (left), total area on the filter paper marked by urine is unchanged (center), and the average urine mark size increases (right). \* $p < 0.05$ ; \*\* $p < 0.01$ ; ns, not significant; Wilcoxon matched-pairs signed rank test.

(D) Inhibiting MPOA Vgat<sup>+</sup> cells (CNO trials) eliminates social-rank-dependent differences in number of urine marks (left) and average urine mark size (right). Mean  $\pm$  SEM. \*\* $p < 0.01$ ; ns, not significant; two-tailed Mann-Whitney *U* test.

### Cellular Composition of the PMC

Single-unit recordings in dorsolateral pons in cats and rats demonstrated the existence of “direct neurons” whose firing rate increases as bladder contracts (de Groat et al., 1998; Sasaki, 2004, 2005). Intermingled with these neurons were “inverse neurons” that could not be stimulated antidromically from spinal cord and whose firing rate decreases as bladder contracts. We find that, in mice, population activity of *Crh*<sup>+</sup> PMC neurons increases with bladder contraction, suggesting that these anatomically and molecularly defined neurons likely correspond to the functionally defined “direct neurons.” Furthermore, we find that in awake and freely moving mice, PMC *Crh*<sup>+</sup> neurons increase activity during urine release, indicating a correlation of their activity not just with bladder contraction but also with micturition, which requires contraction of the bladder wall as well as relaxation of the urinary sphincters. Although not tested here, we hypothesize that “inverse neurons” could correspond to GABAergic *Crh*<sup>−</sup> neurons of the PMC, which may represent inhibitory interneurons.

The elevated activity of direct neurons and of PMC *Crh*<sup>+</sup> neurons during bladder contractions could be caused by ascending sensory signals conveying bladder pressure to the brainstem or could reflect the command signals that trigger bladder contractions. Electrical stimulation in the vicinity of the PMC is sufficient

to trigger bladder contractions in cats (Noto et al., 1989), suggesting the existence of pro-micturition neurons in the pons. We found that ChR2-mediated activation of PMC *Crh*<sup>+</sup> neurons triggered time-locked contraction of the bladder, indicating that activity of these neurons alone is sufficient to trigger bladder contraction. Furthermore, micturating events were triggered with ChR2 stimulations, suggesting that activity of PMC *Crh*<sup>+</sup> neurons is sufficient to trigger both contraction of the detrusor muscle in the bladder wall and relaxation of the urinary sphincters. In addition, although not analyzed here, additional effects of ChR2 stimulation, such as inducing defecation, were occasionally observed, suggesting functional heterogeneity within the PMC *Crh*<sup>+</sup> neurons.

### An Integration Center for Micturition Behavior

If the PMC, and specifically *Crh*<sup>+</sup> neurons of the PMC, mediate complex behavioral control over micturition, they must receive signals from higher brain areas, including those that process olfactory and social hierarchical information. We find that candidate input areas to *Crh*<sup>+</sup> PMC neurons encompass all those previously described to project to the PMC region (Valentino et al., 1999). However, we find additional inputs such as dense projections from cortex (including somatosensory cortex) and motor-related superior colliculus.

Furthermore, whole-brain analysis reveals a widespread micturition regulatory network of at least ~3,500–40,000 neurons, indicating a high degree of convergence onto a maximum of ~500 *Crh*+ PMC neurons. The distribution of candidate presynaptic neurons was similar across animals and of three main classes: olfactory relay nuclei, cerebral cortex, and hypothalamic and brainstem nuclei. Olfactory cues are detected by main olfactory (volatile components) and vomeronasal (non-volatile) systems, which target distinct downstream circuits in the brain (Dulac and Wagner, 2006). Possible olfactory inputs to *Crh*+ neurons arise from main (BSTa, ventral pallidum) and vomeronasal (BSTp) systems, as well as from areas common to both systems (MPOA), suggesting an integration of information from both chemosensory pathways. Urine contains complex sensory signals that include both volatile and non-volatile components, and these findings might explain why mice with genetic ablation of vomeronasal systems have normal micturition pattern in response to female urine but reduced micturition to male urine (Kaur et al., 2014; Leybold et al., 2002; Maruniak et al., 1986), as the former might rely mostly on the main olfactory system and the latter on the vomeronasal system. Potential shortest paths (Dulac and Torello, 2003; Kang et al., 2011) to reach the PMC from the nose are main olfactory bulb (MOB) → medial amygdalar nucleus (MeA) → BSTa/MPOA → PMC (for the main olfactory system) and accessory olfactory bulb (AOB) → BSTp/MPOA → PMC (for the vomeronasal system). *Crh*+ PMC neurons also receive extensive projections from dorsal medial prefrontal cortex, including ACA and PL, regions that encode and causally affect social rank in rodents (Holson, 1986; Wang et al., 2011).

This complex and multi-modal set of projections to *Crh*+ PMC neurons reaffirms that they likely constitute the control center that integrates olfactory and social hierarchical information to regulate micturition. Coupled with our findings that PMC *Crh*+ neurons are direct regulators of micturition, these results provide an anatomical and molecular entry point into dissecting the decision-making process for context-dependent micturition behavior. The whole-brain survey of candidate input regions to PMC *Crh*+ neurons reveals inputs from areas of unclear function and may illuminate additional factors that regulate micturition, as well as inform possible mechanisms for bladder dysfunction in diseases of the CNS.

## STAR★METHODS

Detailed methods are provided in the online version of this paper and include the following:

- KEY RESOURCES TABLE
- CONTACT FOR REAGENT AND RESOURCE SHARING
- EXPERIMENTAL MODEL AND SUBJECT DETAILS
  - Mice
- METHOD DETAILS
  - Behavioral Assays and Analyses
  - Acute Brain Slice Preparation and Electrophysiology
  - Virus Preparation
  - Stereotaxic Intracranial Injections and Optic Fiber Implant

- In Vivo Cystometry Surgery and Measurement with Optogenetic Activation
- In Vivo Fiber Photometry Recordings and Analysis
- In Vivo Neuronal Silencing in PMC and MPOA
- Immunohistochemistry and RNA In Situ Hybridization
- Rabies-Based Retrograde *Trans*-synaptic Tracing with Serial Two-Photon Tomography

## ● QUANTIFICATION AND STATISTICAL ANALYSIS

## SUPPLEMENTAL INFORMATION

Supplemental Information includes seven figures, one table, and two movies and can be found with this article online at <http://dx.doi.org/10.1016/j.cell.2016.08.073>.

## AUTHOR CONTRIBUTIONS

X.H.H., M.H., J.T., P.O., and B.L.S. designed and directed experiments; X.H.H., M.H., J.T., E.T., D.F., E.A., and D.C. performed experiments; X.H.H., M.H., and J.T. analyzed data; K.W.H. generated and validated the rabies virus; M.L.Z. advised on cystometry experiments; X.H.H. and B.L.S. conceived of the project and wrote the paper with contributions from M.H.

## ACKNOWLEDGMENTS

We thank R. Pemberton and J. Levasseur for genotyping and animal husbandry; J. Saulnier, L. Glick, T. Haynes, D. Rothfuss, and A. Strasser for technical support; D. Strohlic and A. Saunders for help generating the AAV-DIO-PLAP construct; Z. Wu for help with in situ hybridization; L. Guo and J. Mathai for help with cystometry; L. Ding for assistance with image analysis; I. Oldenburg, D. Roberson, O. Mazor, and P. Gorelik for advice on the behavioral arena; J.N. Betley for advice on chemogenetic experiments; M. Wallace for blinding experimental conditions for quantifications and analyses; and S.R. Datta, Y. Kozorovitskiy, and members of the laboratories for helpful discussions and comments on the manuscript. Starting materials for generating pseudotyped rabies virus were a generous gift from B.K. Lim (UC San Diego). Confocal images were acquired at the Harvard Neurobiology Imaging Facility (NIH P30NS072030) and Harvard NeuroDiscovery Imaging Core. This work was supported by a Stuart H.Q. and Victoria Quan Fellowship (X.H.H.), by a Samsung Scholarship (M.H.), and by the NIH (grant P20DK103086 to M.L.Z. and B.L.S. and grants R01MH096946 and U01MH105971 to P.O.).

Received: February 25, 2016

Revised: June 28, 2016

Accepted: August 23, 2016

Published: September 22, 2016

## REFERENCES

- Bacchini, A., Gaetani, E., and Cavaggioni, A. (1992). Pheromone binding proteins of the mouse, *Mus musculus*. *Experientia* 48, 419–421.
- Barrington, F.J.F. (1925). The effect of lesions of the hind- and mid-brain on micturition in the cat. *Exp. Physiol.* 15, 81–102.
- Betts, C.D., Kapoor, R., and Fowler, C.J. (1992). Pontine pathology and voiding dysfunction. *Br. J. Urol.* 70, 100–102.
- Beynon, R.J., Veggerby, C., Payne, C.E., Robertson, D.H.L., Gaskell, S.J., Humphries, R.E., and Hurst, J.L. (2002). Polymorphism in major urinary proteins: molecular heterogeneity in a wild mouse population. *J. Chem. Ecol.* 28, 1429–1446.
- Blok, B.F.M., and Holstege, G. (1998). The central nervous system control of micturition in cats and humans. *Behav. Brain Res.* 92, 119–125.
- Blok, B.F.M., and Holstege, G. (2000). The pontine micturition center in rat receives direct lumbosacral input. An ultrastructural study. *Neurosci. Lett.* 282, 29–32.

- Brennan, P.A., and Keverne, E.B. (2004). Something in the air? New insights into mammalian pheromones. *Curr. Biol.* *14*, R81–R89.
- Chen, T.-W., Wardill, T.J., Sun, Y., Pulver, S.R., Renninger, S.L., Baohan, A., Schreiter, E.R., Kerr, R.A., Orger, M.B., Jayaraman, V., et al. (2013). Ultrasensitive fluorescent proteins for imaging neuronal activity. *Nature* *499*, 295–300.
- Cui, G., Jun, S.B., Jin, X., Pham, M.D., Vogel, S.S., Lovinger, D.M., and Costa, R.M. (2013). Concurrent activation of striatal direct and indirect pathways during action initiation. *Nature* *494*, 238–242.
- de Groat, W.C., and Wickens, C. (2013). Organization of the neural switching circuitry underlying reflex micturition. *Acta Physiol. (Oxf.)* *207*, 66–84.
- de Groat, W.C., Araki, I., Vizzard, M.A., Yoshiyama, M., Yoshimura, N., Sugaya, K., Tai, C., and Roppolo, J.R. (1998). Developmental and injury induced plasticity in the micturition reflex pathway. *Behav. Brain Res.* *92*, 127–140.
- Desjardins, C., Maruniak, J.A., and Bronson, F.H. (1973). Social rank in house mice: differentiation revealed by ultraviolet visualization of urinary marking patterns. *Science* *182*, 939–941.
- Ding, Y.Q., Zheng, H.X., Gong, L.W., Lu, Y., Zhao, H., and Qin, B.Z. (1997). Direct projections from the lumbosacral spinal cord to Barrington's nucleus in the rat: a special reference to micturition reflex. *J. Comp. Neurol.* *389*, 149–160.
- Drake, M.J., Fowler, C.J., Griffiths, D., Mayer, E., Paton, J.F., and Birder, L. (2010). Neural control of the lower urinary and gastrointestinal tracts: supraspinal CNS mechanisms. *NeuroUrol. Urodyn.* *29*, 119–127.
- Dulac, C., and Torello, A.T. (2003). Molecular detection of pheromone signals in mammals: from genes to behaviour. *Nat. Rev. Neurosci.* *4*, 551–562.
- Dulac, C., and Wagner, S. (2006). Genetic analysis of brain circuits underlying pheromone signaling. *Annu. Rev. Genet.* *40*, 449–467.
- Ewer, R.F. (1968). *Ethology of Mammals* (Plenum Press).
- Fowler, C.J., Griffiths, D., and de Groat, W.C. (2008). The neural control of micturition. *Nat. Rev. Neurosci.* *9*, 453–466.
- Franklin, K.B.J., and Paxinos, G. (2007). *The Mouse Brain in Stereotaxic Coordinates*, Third Edition (Academic Press).
- Gunaydin, L.A., Grosenick, L., Finkelstein, J.C., Kauvar, I.V., Fenno, L.E., Adhikari, A., Lammel, S., Mirzabekov, J.J., Airan, R.D., Zalocusky, K.A., et al. (2014). Natural neural projection dynamics underlying social behavior. *Cell* *157*, 1535–1551.
- Henderleiter, J.A., and Hyslop, R.M. (1996). The analysis of riboflavin in urine using fluorescence. *J. Chem. Educ.* *73*, 563.
- Holson, R.R. (1986). Mesial prefrontal cortical lesions and timidity in rats. III. Behavior in a semi-natural environment. *Physiol. Behav.* *37*, 239–247.
- Holstege, G., Griffiths, D., de Wall, H., and Dalm, E. (1986). Anatomical and physiological observations on supraspinal control of bladder and urethral sphincter muscles in the cat. *J. Comp. Neurol.* *250*, 449–461.
- Hurst, J.L., and Beynon, R.J. (2004). Scent wars: the chemobiology of competitive signalling in mice. *BioEssays* *26*, 1288–1298.
- Hurst, J.L., Robertson, D.H.L., Tolladay, U., and Beynon, R.J. (1998). Proteins in urine scent marks of male house mice extend the longevity of olfactory signals. *Anim. Behav.* *55*, 1289–1297.
- Kang, N., Baum, M.J., and Cherry, J.A. (2011). Different profiles of main and accessory olfactory bulb mitral/tufted cell projections revealed in mice using an anterograde tracer and a whole-mount, flattened cortex preparation. *Chem. Senses* *36*, 251–260.
- Kaur, A.W., Ackels, T., Kuo, T.-H., Cichy, A., Dey, S., Hays, C., Kateri, M., Logan, D.W., Marton, T.F., Spehr, M., and Stowers, L. (2014). Murine pheromone proteins constitute a context-dependent combinatorial code governing multiple social behaviors. *Cell* *157*, 676–688.
- Keegan, C.E., Karolyi, I.J., Knapp, L.T., Bourbonnais, F.J., Camper, S.A., and Seasholtz, A.F. (1994). Expression of corticotropin-releasing hormone transgenes in neurons of adult and developing mice. *Mol. Cell. Neurosci.* *5*, 505–514.
- Kim, Y., Venkataraju, K.U., Pradhan, K., Mende, C., Taranda, J., Turaga, S.C., Arganda-Carreras, I., Ng, L., Hawrylycz, M.J., Rockland, K.S., et al. (2015). Mapping social behavior-induced brain activation at cellular resolution in the mouse. *Cell Rep.* *10*, 292–305.
- Klein, S., Staring, M., Murphy, K., Viergever, M.A., and Pluim, J.P.W. (2010). elastix: a toolbox for intensity-based medical image registration. *IEEE Trans. Med. Imaging* *29*, 196–205.
- Leypold, B.G., Yu, C.R., Leinders-Zufall, T., Kim, M.M., Zufall, F., and Axel, R. (2002). Altered sexual and social behaviors in *trp2* mutant mice. *Proc. Natl. Acad. Sci. USA* *99*, 6376–6381.
- Lindzey, G., Winston, H., and Manosevitz, M. (1961). Social dominance in inbred mouse strains. *Nature* *191*, 474–476.
- Madisen, L., Zwingman, T.A., Sunkin, S.M., Oh, S.W., Zariwala, H.A., Gu, H., Ng, L.L., Palmiter, R.D., Hawrylycz, M.J., Jones, A.R., et al. (2010). A robust and high-throughput Cre reporting and characterization system for the whole mouse brain. *Nat. Neurosci.* *13*, 133–140.
- Mallory, B.S., Roppolo, J.R., and de Groat, W.C. (1991). Pharmacological modulation of the pontine micturition center. *Brain Res.* *546*, 310–320.
- Maruniak, J.A., Wysocki, C.J., and Taylor, J.A. (1986). Mediation of male mouse urine marking and aggression by the vomeronasal organ. *Physiol. Behav.* *37*, 655–657.
- Miyamichi, K., Shlomal-Fuchs, Y., Shu, M., Weissbourd, B.C., Luo, L., and Mizrahi, A. (2013). Dissecting local circuits: parvalbumin interneurons underlie broad feedback control of olfactory bulb output. *Neuron* *80*, 1232–1245.
- Noto, H., Roppolo, J.R., Steers, W.D., and de Groat, W.C. (1989). Excitatory and inhibitory influences on bladder activity elicited by electrical stimulation in the pontine micturition center in the rat. *Brain Res.* *492*, 99–115.
- Ragan, T., Kadiri, L.R., Venkataraju, K.U., Bahlmann, K., Sutin, J., Taranda, J., Arganda-Carreras, I., Kim, Y., Seung, H.S., and Osten, P. (2012). Serial two-photon tomography for automated ex vivo mouse brain imaging. *Nat. Methods* *9*, 255–258.
- Ralls, K. (1971). Mammalian scent marking. *Science* *171*, 443–449.
- Rouzade-Dominguez, M.-L., Pernar, L., Beck, S., and Valentino, R.J. (2003). Convergent responses of Barrington's nucleus neurons to pelvic visceral stimuli in the rat: a juxtacellular labelling study. *Eur. J. Neurosci.* *18*, 3325–3334.
- Sasaki, M. (2004). Feed-forward and feedback regulation of bladder contractility by Barrington's nucleus in cats. *J. Physiol.* *557*, 287–305.
- Sasaki, M. (2005). Role of Barrington's nucleus in micturition. *J. Comp. Neurol.* *493*, 21–26.
- Simerly, R.B., and Swanson, L.W. (1986). The organization of neural inputs to the medial preoptic nucleus of the rat. *J. Comp. Neurol.* *246*, 312–342.
- Simerly, R.B., and Swanson, L.W. (1988). Projections of the medial preoptic nucleus: a Phaseolus vulgaris leucoagglutinin anterograde tract-tracing study in the rat. *J. Comp. Neurol.* *270*, 209–242.
- Simerly, R.B., Gorski, R.A., and Swanson, L.W. (1986). Neurotransmitter specificity of cells and fibers in the medial preoptic nucleus: an immunohistochemical study in the rat. *J. Comp. Neurol.* *246*, 343–363.
- Singer, A.G., Beauchamp, G.K., and Yamazaki, K. (1997). Volatile signals of the major histocompatibility complex in male mouse urine. *Proc. Natl. Acad. Sci. USA* *94*, 2210–2214.
- Sugaya, K., Roppolo, J.R., Yoshimura, N., Card, J.P., and de Groat, W.C. (1997). The central neural pathways involved in micturition in the neonatal rat as revealed by the injection of pseudorabies virus into the urinary bladder. *Neurosci. Lett.* *223*, 197–200.
- Sugaya, K., Ogawa, Y., Hatano, T., Nishijima, S., Matsuyama, K., and Mori, S. (2003). Ascending and descending brainstem neuronal activity during cystometry in decerebrate cats. *NeuroUrol. Urodyn.* *22*, 343–350.
- Sunkin, S.M., Ng, L., Lau, C., Dolbeare, T., Gilbert, T.L., Thompson, C.L., Hawrylycz, M., and Dang, C. (2013). Allen Brain Atlas: an integrated spatio-temporal portal for exploring the central nervous system. *Nucleic Acids Res.* *41*, D996–D1008.
- Takasaki, A., Hui, M., and Sasaki, M. (2010). Is the periaqueductal gray an essential relay center for the micturition reflex pathway in the cat? *Brain Res.* *1377*, 108–115.

- Tamamaki, N., Yanagawa, Y., Tomioka, R., Miyazaki, J., Obata, K., and Kamekura, T. (2003). Green fluorescent protein expression and colocalization with calretinin, parvalbumin, and somatostatin in the GAD67-GFP knock-in mouse. *J. Comp. Neurol.* *467*, 60–79.
- Tanaka, Y., Koyama, Y., Kayama, Y., Kawauchi, A., Ukimura, O., and Miki, T. (2003). Firing of micturition center neurons in the rat mesopontine tegmentum during urinary bladder contraction. *Brain Res.* *965*, 146–154.
- Taniguchi, H., He, M., Wu, P., Kim, S., Paik, R., Sugino, K., Kvitsiani, D., Fu, Y., Lu, J., Lin, Y., et al. (2011). A resource of Cre driver lines for genetic targeting of GABAergic neurons in cerebral cortex. *Neuron* *71*, 995–1013.
- Turaga, S.C., Murray, J.F., Jain, V., Roth, F., Helmstaedter, M., Briggman, K., Denk, W., and Seung, H.S. (2010). Convolutional networks can learn to generate affinity graphs for image segmentation. *Neural Comput.* *22*, 511–538.
- Uvin, P., Everaerts, W., Pinto, S., Alpizar, Y.A., Boudes, M., Gevaert, T., Voets, T., Nilius, B., Talavera, K., and De Ridder, D. (2012). The use of cystometry in small rodents: a study of bladder chemosensation. *J. Vis. Exp.* *66*, e3869.
- Valentino, R.J., Page, M.E., Luppi, P.-H., Zhu, Y., Van Bockstaele, E., and Aston-Jones, G. (1994). Evidence for widespread afferents to Barrington's nucleus, a brainstem region rich in corticotropin-releasing hormone neurons. *Neuroscience* *62*, 125–143.
- Valentino, R.J., Chen, S., Zhu, Y., and Aston-Jones, G. (1996). Evidence for divergent projections to the brain noradrenergic system and the spinal parasympathetic system from Barrington's nucleus. *Brain Res.* *732*, 1–15.
- Valentino, R.J., Miselis, R.R., and Pavcovich, L.A. (1999). Pontine regulation of pelvic viscera: pharmacological target for pelvic visceral dysfunctions. *Trends Pharmacol. Sci.* *20*, 253–260.
- Valentino, R.J., Kosboth, M., Colflesh, M., and Miselis, R.R. (2000). Transneuronal labeling from the rat distal colon: anatomic evidence for regulation of distal colon function by a pontine corticotropin-releasing factor system. *J. Comp. Neurol.* *417*, 399–414.
- Vincent, S.R., and Satoh, K. (1984). Corticotropin-releasing factor (CRF) immunoreactivity in the dorsolateral pontine tegmentum: further studies on the micturition reflex system. *Brain Res.* *308*, 387–391.
- Vong, L., Ye, C., Yang, Z., Choi, B., Chua, S., Jr., and Lowell, B.B. (2011). Leptin action on GABAergic neurons prevents obesity and reduces inhibitory tone to POMC neurons. *Neuron* *71*, 142–154.
- Wall, N.R., Wickersham, I.R., Cetin, A., De La Parra, M., and Callaway, E.M. (2010). Monosynaptic circuit tracing in vivo through Cre-dependent targeting and complementation of modified rabies virus. *Proc. Natl. Acad. Sci. USA* *107*, 21848–21853.
- Wang, F., Zhu, J., Zhu, H., Zhang, Q., Lin, Z., and Hu, H. (2011). Bidirectional control of social hierarchy by synaptic efficacy in medial prefrontal cortex. *Science* *334*, 693–697.
- Wickersham, I.R., Lyon, D.C., Barnard, R.J.O., Mori, T., Finke, S., Conzelmann, K.-K., Young, J.A.T., and Callaway, E.M. (2007). Monosynaptic restriction of transsynaptic tracing from single, genetically targeted neurons. *Neuron* *53*, 639–647.
- Wickersham, I.R., Sullivan, H.A., and Seung, H.S. (2010). Production of glycoprotein-deleted rabies viruses for monosynaptic tracing and high-level gene expression in neurons. *Nat. Protoc.* *5*, 595–606.
- Willette, R.N., Morrison, S., Sapru, H.N., and Reis, D.J. (1988). Stimulation of opiate receptors in the dorsal pontine tegmentum inhibits reflex contraction of the urinary bladder. *J. Pharmacol. Exp. Ther.* *244*, 403–409.
- Wu, Z., Autry, A.E., Bergan, J.F., Watabe-Uchida, M., and Dulac, C.G. (2014). Galanin neurons in the medial preoptic area govern parental behaviour. *Nature* *509*, 325–330.
- Yamaguchi, M., Yamazaki, K., Beauchamp, G.K., Bard, J., Thomas, L., and Boyse, E.A. (1981). Distinctive urinary odors governed by the major histocompatibility locus of the mouse. *Proc. Natl. Acad. Sci. USA* *78*, 5817–5820.
- Yamazaki, K., Beauchamp, G.K., Egorov, I.K., Bard, J., Thomas, L., and Boyse, E.A. (1983). Sensory distinction between H-2b and H-2bm1 mutant mice. *Proc. Natl. Acad. Sci. USA* *80*, 5685–5688.

## STAR★METHODS

## KEY RESOURCES TABLE

REAGENT or RESOURCE	SOURCE	IDENTIFIER
<b>Antibodies</b>		
Rabbit polyclonal anti-NeuN	Millipore	Cat# ABN78; RRID: AB_10807945
Rabbit polyclonal anti-tyrosine-hydroxylase	Millipore	Cat# AB152; RRID: AB_390204
Rabbit polyclonal anti-c-Fos	Santa Cruz	Cat# SC52; RRID: AB_10160513
Goat monoclonal anti-rabbit IgG secondary antibody, Alexa Fluor 488 conjugate	Invitrogen	Cat# A-11034
<b>Chemicals, Peptides, and Recombinant Proteins</b>		
Picrotoxin	Tocris	Cat# 1128
NBQX	Tocris	Cat# 0373
CPP	Tocris	Cat# 0247
Digoxigenin RNA Labeling Mix	Roche	Cat# 11277073910
Fluorescein RNA Labeling Mix	Roche	Cat# 11685619910
Dinitrophenyl RNA labeling mix	Perkin Elmer	Cat# NEL555
<b>Critical Commercial Assays</b>		
RNAscope Multiplex Fluorescent Reagent Kit	Advanced Cell Diagnostics	Cat# 320850
TSA Plus Cyanine 3 System	Perkin Elmer	Cat# NEL744
<b>Experimental Models: Organisms/Strains</b>		
Mouse: C57BL/6N	Charles River	Cat# 027
Mouse: B6(Cg)-Crrh <sup>tm1(cre)Zjh</sup> /J	Jackson Laboratory (Taniguchi et al., 2011)	Cat# 012704
Mouse: B6.Cg-Gt(ROSA)26Sor <sup>tm14(CAG-tdTomato)Hze</sup> /J	Jackson Laboratory (Madisen et al., 2010)	Cat# 007914
Mouse: B6.Cg-Gt(ROSA)26Sor <sup>tm6(CAG-ZsGreen1)Hze</sup> /J	Jackson Laboratory (Madisen et al., 2010)	Cat# 007906
Mouse: <i>Gad1</i> <sup>ires-GFP</sup>	Tamamaki et al. (2003)	N/A
Mouse: <i>Gad2</i> <sup>tm2(cre)Zjh</sup> /J	Jackson Laboratory (Taniguchi et al., 2011)	Cat# 010802
Mouse: <i>Slc32a1</i> <sup>tm2(cre)Lowl</sup> /J	Jackson Laboratory (Vong et al., 2011)	Cat# 016962
Mouse: <i>Slc17a6</i> <sup>tm2(cre)Lowl</sup> /J	Jackson Laboratory (Vong et al., 2011)	Cat# 016963
<b>Recombinant DNA</b>		
AAV2/9-CAG-DIO-PLAP	This paper	Addgene# 81244
AAV2/9-CBA-DIO-hM4Di-mCherry	This paper	Addgene# 81008
AAV2/9-CAG-DIO-TVA-mCherry	Miyamichi et al., 2013	Addgene# 48332
AAV2/9-CAG-DIO-RG	Miyamichi et al., 2013	Addgene# 48333
AAV2/9-CAG-DIO-GCaMP6s-WPRE	Penn Vector Core	Cat# AV-9-PV2833
AAV2/9-CAG-Flex-tdTomato-WPRE	Penn Vector Core	Cat# AV-1-ALL864
AAV2/9-CAGGS-Flex-ChR2-tdTomato-WPRE	Penn Vector Core	Cat# AV-9-18917P
AAV2/8-Elfx-DIO-hM4Di-mCherry	Addgene	Addgene# 50461
<b>Software and Algorithms</b>		
Urine pattern analysis code	This paper	<a href="https://github.com/bernardosabatinilab">https://github.com/bernardosabatinilab</a>
Elastix, intensity-based image registration	Klein et al., 2010	N/A
Convolutional networks trained to recognize EGFP-positive neurons	Turaga et al., 2010	N/A
Mouse position video tracking software	Noldus	Cat # Ethovision XT
<b>Other</b>		
Chromatography Paper	Whatman	Cat# 05-714-5

## CONTACT FOR REAGENT AND RESOURCE SHARING

Further information and requests for reagents may be directed to, and will be fulfilled by, the corresponding author Bernardo L. Sabatini ([bsabatini@hms.harvard.edu](mailto:bsabatini@hms.harvard.edu)).

## EXPERIMENTAL MODEL AND SUBJECT DETAILS

### Mice

Animals were group housed unless for behavior experiments (see below), maintained with food and water available *ad libitum* and on a 12 hr/12 hr light/dark cycle (dark hours: 10:00–22:00). Knock-in mice with an internal ribosome entry site (ires)-linked Cre recombinase gene downstream of the *Crh* locus (*Crh*<sup>ires-Cre</sup> mice, Jackson Laboratory # 012704) (Taniguchi et al., 2011) were crossed with Cre-dependent tdTomato (Ai14, Jackson Labs # 007914, referred to as *Rosa26*<sup>Isl-tdTomato</sup>) or ZsGreen1 (Ai6, Jackson Labs # 007906, referred to as *Rosa26*<sup>Isl-zsGreen</sup>) reporter mice to visualize Cre-positive cells (Madisen et al., 2010). *Gad1*<sup>ires-GFP</sup> (Tamamaki et al., 2003), *Gad2*<sup>ires-Cre</sup> (Taniguchi et al., 2011), *Slc32a1*<sup>ires-Cre</sup>, and *Slc17a6*<sup>ires-Cre</sup> (Vong et al., 2011) were also used for cell type identifications of glutamic acid decarboxylase 1 (GAD1), glutamic acid decarboxylase 2 (GAD2), vesicular GABA transporter (VGAT) or vesicular glutamate transporter 2 (VGLUT2)-positive cells, respectively.

With the exception of *Slc32a1*<sup>ires-Cre</sup> and *Slc17a6*<sup>ires-Cre</sup> mice, which were maintained on a mixed background, all other strains were maintained on a C57BL/6N background. All experimental manipulations were performed in accordance with protocols approved by the Harvard Standing Committee on Animal Care following guidelines described in the National Institutes of Health Guide for the Care and Use of Laboratory Animals.

## METHOD DETAILS

### Behavioral Assays and Analyses

Pair-housed adult wild-type C57BL/6N male mice were separated into individual fresh cages (with food supply but no water supply) lined with filter paper (28 × 11 cm, Whatman #05-714-5) with an olfactory stimulus (100  $\mu$ l estrous female urine or saline) added to the center and rubbed onto the nose of the mice. Female urine was freshly collected and pooled from urine of 4–5 estrous females. After two hours in the arena, mice were removed, tested for social hierarchy with their previous cage mate using the tube test as described previously (Lindzey et al., 1961; Wang et al., 2011). Briefly, two cage mates were simultaneously released into the opposite ends of a plastic tube (3cm diameter, 30cm length), and the mouse that retreated from the tube first was designated as subordinate. Afterward, the brains were processed for histology as described below. In parallel, the distribution of urine spots on the paper was examined with fluorescence imaging. In response to blue light excitation, urine marks deposited on filter paper have a slightly red-shifted fluorescent emission spectrum compared to previously described emission profile of urine, which was largely attributed to riboflavin (Henderleiter and Hyslop, 1996); we therefore used blue LED light excitation (peak centered at 473nm) with a GFP filter set (excitation at  $472 \pm 25$ nm and emission at  $520 \pm 25$ nm, Semrock).

The distribution, number, and size of urine marks were quantified blind to experimental conditions. To quantify spatial distribution of urine marks throughout the cage, the urine mark image was thresholded and converted into a mask, which was used to calculate the distance distribution of all urine-covered pixels to the stimulus center. The number of urine marks and boundary of each urine mark were determined with a custom ImageJ macro and manually validated spot-by-spot. The cumulative distribution of urine mark size was calculated based on the boundary of each urine mark, binned in 100-pixel intervals (250 bins total), smoothed over a 10-bin span with a box filter, and converted to  $\text{cm}^2$ .

### Acute Brain Slice Preparation and Electrophysiology

Acute brain slices were obtained from 17- to 21-day-old *Crh*<sup>ires-Cre::Rosa26</sup><sup>Isl-tdTomato</sup> mice using standard techniques. Mice were anaesthetized by isoflurane inhalation and the brainstem was removed, 190  $\mu$ m coronal slices were cut in cold choline-based cutting solution (consisting of (in mM): 110 choline chloride, 25  $\text{NaHCO}_3$ , 2.5 KCl, 7  $\text{MgCl}_2$ , 0.5  $\text{CaCl}_2$ , 1.25  $\text{NaH}_2\text{PO}_4$ , 25 glucose, 11.6 ascorbic acid, and 3.1 pyruvic acid) with a Leica VT1000s vibratome, transferred for 20 min to a holding chamber containing ACSF, consisting of (in mM) 125 NaCl, 2.5 KCl, 25  $\text{NaHCO}_3$ , 2  $\text{CaCl}_2$ , 1  $\text{MgCl}_2$ , 1.25  $\text{NaH}_2\text{PO}_4$ , and 11 glucose (300  $\text{mOsm kg}^{-1}$ ) at 34 °C and subsequently maintained at room temperature (20–22 °C) until use. All recordings were obtained within 5 hr of slicing. Both cutting solution and ACSF were constantly bubbled with 95%  $\text{O}_2$ /5%  $\text{CO}_2$ .

Whole-cell current-clamp recordings were obtained at 34 °C. A cocktail of neurotransmitter receptor antagonists was applied (AMPA- and NMDA-type glutamate receptor antagonists NBQX and CPP, respectively; GABAA and glycine receptor antagonist picrotoxin) to block ionotropic synaptic transmission. Drugs (all from Tocris) were applied by bath perfusion; picrotoxin (10  $\mu$ M), NBQX (10  $\mu$ M), CPP (10  $\mu$ M). Patch pipettes (2–4 M $\Omega$ ) pulled from borosilicate glass (G150F-3, Warner Instruments) were filled with a  $\text{K}^+$ -based low  $\text{Cl}^-$  internal solution composed of (in mM) 135 KMeSO<sub>3</sub>, 3 KCl, 10 HEPES, 1 EGTA, 0.1  $\text{CaCl}_2$ , 4 Mg-ATP, 0.3 Na-GTP, 8 Na<sub>2</sub>-phosphocreatine (pH 7.3 adjusted with KOH; 295  $\text{mOsm} \cdot \text{kg}^{-1}$ ) for current-clamp recordings.

*Crh*<sup>+</sup> and *Crh*<sup>-</sup> cells were distinguished based on tdTomato fluorescence. Passive and active cellular properties were measured and compared across the populations. Steps of positive current were injected to obtain current-to-firing rate relationships (IF curves),

and steps of negative current to calculate membrane resistance ( $R_m$ ), capacitance ( $C_m$ ), and time constant ( $\tau$ ). Action potential width (full width at half maximum, FWHM) and the amplitude of sag potential (sag amp., typically mediated by hyperpolarization-activated cyclic nucleotide gated channels and the associated cationic current  $I_h$ ). Spontaneous firing rates (spont.  $f$ ) were measured in whole-cell configuration with  $K^+$ -based internal solution without current injection, the results of which were consistent with measurements in cell-attached configuration with artificial cerebral spinal fluid (ACSF) in the recording pipette (Figure S2B).

### Virus Preparation

Serotype 2.9 recombinant AAV vectors for AAV-DIO-PLAP, AAV-DIO-hM4Di-mCherry, AAV-DIO-TVA-mCherry and AAV-DIO-RG were produced by commercial vector core facilities (University of North Carolina and Boston Children's Hospital), whereas AAV-DIO-GCaMP6s (AAV9.CAG.GCaMP6s.WPRE.SV40), AAV-DIO-tdTomato (AAV9.CAG.Flex. tdTomato.WPRE.bGH, Allen Institute 864), and AAV-DIO-ChR2-tdTomato (AAV9.CAGGS.Flex.ChR2-tdTomato.WPRE.SV40, Addgene 18917) were obtained from University of Pennsylvania vector core. All AAVs were used at a genomic titer of approximately  $1.3 \times 10^{13}$  viral particles per ml. Although not systematically tested, attempts to obtain robust expression of transgenes in PMC *Crh* neurons with other AAV serotypes and promoters were not successful.

EnvA-pseudotyped, glycoprotein-deleted rabies virus carrying EGFP transgene (RbV-EGFP) was generated in house, using starting materials from Byungkook Lim (UCSD). The recombinant rabies viruses were generated using BHK-B19G and BHK-EnvA cells using protocols similar to those previously described (Wickersham et al., 2010) and were used at a titer of approximately  $1.0 \times 10^9$  infectious units/ml.

### Stereotaxic Intracranial Injections and Optic Fiber Implant

To target PMC *Crh*+ neurons, *Crh*<sup>ires-cre</sup> male mice (P55-60) were anaesthetized with isoflurane and placed in a small animal stereotaxic frame (David Kopf Instruments). After exposing the skull under aseptic conditions, a small burr hole was drilled and AAVs were injected (150-500 nl total volume) unilaterally through a pulled glass pipette at a rate of  $120 \text{ nl min}^{-1}$ . Injection coordinates for PMC were 5.25 mm posterior from Bregma, 0.70 mm lateral and 3.6 mm below pia. Similarly, to target MPOA *Vgat*+ neurons, AAVs were bilaterally injected (800 nl on each side) into *Slc32a1*<sup>ires-Cre</sup> mice with injection coordinate of 0.00 mm posterior from Bregma, 0.50 mm lateral and 5.0 mm below pia. After surgical procedures, all mice were returned to their home cage for at least 21 days to allow recovery and to maximize gene expression.

For photometry measurement and optogenetic stimulation experiments, a second surgery took place after 21 days of injection, where an optic fiber (200  $\mu\text{m}$  inner core diameter; 0.22 NA for photometry measurement, Doric Lenses; 0.39 NA for optogenetics stimulation, Thorlabs) was implanted above PMC (5.25 mm posterior from Bregma, 0.70 mm lateral and 3.4 mm below pia) and affixed to the skull with dental cement. Mice were allowed to recover for at least 7 days after implantation.

For rabies virus injections, a second surgery took place 21 days after the first injection (150 nl of a 1:1 mixture of AAV-DIO-TVA-mCherry and AAV-DIO-RG) at which 350 nl of RbV-EGFP was injected into PMC as described above. Mice were euthanized after 7 days in a biosafety level 2 animal facility.

### In Vivo Cystometry Surgery and Measurement with Optogenetic Activation

*Crh*<sup>ires-cre</sup> male mice with AAV-DIO-ChR2-tdTomato or AAV-DIO-tdTomato (as control) injected into PMC and optic fiber implanted above PMC underwent cystometry surgery. Catheter (PE10) was secured purse-string style into the bladder. Measurements were done under urethane anesthesia and with saline infusion into the catheter at 40  $\mu\text{l/min}$ . Light from a 473 nm laser (Ciel, Laser Quantum) was delivered in 15 ms pulses at 20 Hz for 5 s. The light train was delivered once every 60 s for fixed-interval stimulation, or at randomized intervals between 30 s and 90 s. The light power exiting the fiber tip was at 10-20 mW, ensuring a light intensity above  $1 \text{ mW/mm}^2$  over the entire PMC.

### In Vivo Fiber Photometry Recordings and Analysis

The bulk fluorescence acquisition setup consisted of a 473 nm laser (Ciel, Laser Quantum) for excitation of the fluorophore, which was attenuated with absorptive neutral density filters (OD = 0-2.0, Thorlabs NDM2). The optics consisted of an excitation filter (Semrock FF02-482/18), a sequence of lenses for expanding the laser beam and focusing it onto the fiber entry ( $F = -25\text{mm}$ , 75mm, 25mm, Edmund Optics #45-922 #63-809, #47-342), and a dichroic mirror for separation of excitation and emission wavelengths (Semrock Di02-R488), an emission filter (Semrock FF03-525/50) and a lens ( $F = 25\text{mm}$ , Edmund Optics #47-342) to focus onto the photomultiplier tube (Hamamatsu H7422-40). For two-color bulk fluorescence recording, an additional 561 nm laser (gem, Laser Quantum) was used for excitation of the red fluorophore with the additional focusing lens, filters and dichroic mirrors (Doric Lenses, FMC2). The red signal was independently collected with a photomultiplier tube (Hamamatsu H7422-40). The light power exiting the fiber tip was at 10  $\mu\text{W}$ .

For both anesthetized and awake freely moving recordings, the relative change in fluorescence,  $\Delta F/F = (F - F_0)/F_0$  was calculated for each session with  $F_0$  as 10th percentile of a 20 s running window to correct for drift fluorescence. To create shuffled photometry data, we divided the original data into 10 min segments and then randomly associated segments of photometry data with segments of cystometry data. An analogous approach was used to randomly associate photometry and urine marking behavior. This method preserves the natural statistics of each signal on the relevant timescale of the analysis.

Specifically for anesthetized simultaneous recordings, data acquisition channels on DAQ for photometry and cystometry were interleaved with control channels to rule out that the correlation observed was an artifact of electric crosstalk between data acquisition channels. For cross-correlation analysis, bladder pressure and fluorescence signals were rescaled to have mean = 0 and standard deviation = 1 to generate two z-scored time-varying signals. Cross-correlations were calculated with *xcorr* in Matlab (MathWorks) with the peak of the value of cross-correlation reported.

For freely-moving recordings, urine deposits (as described above) and position of the animal (PhenoTyper and Ethovision XT, Noldus) were tracked in real-time in a custom-made arena (26x26 cm). Instead of female urine at the center of arena, intraperitoneal injection of the diuretic furosemide (40 mg/kg) was used to increase the number of micturition events per session. Time stamps from urine spot-tracking video frames and from fiber photometry were acquired with the same data acquisition board to synchronize the data.

### In Vivo Neuronal Silencing in PMC and MPOA

To silence *Crh*+ PMC neurons, pair-housed *Crh<sup>ires-cre</sup>::Rosa26<sup>lsI-zsGreen</sup>* male mice were bilateral injected with AAV-DIO-hM4Di-mCherry (AAV2/9-CBA-DIO-hM4Di-mCherry) into PMC (as described above) and allowed 3 weeks of recovery. One week before behavioral testing, mice were habituated to unrestrained mock intraperitoneal (IP) injection of saline to reduce stress caused by handling and IP injection. Mice were then subjected to two cycles of behavioral testing. Each cycle contained one trial with CNO IP injection, and one trial with saline IP injection, in random order and separated by 3–4 days. For each behavioral trial, mice underwent IP injection of CNO or saline and were returned to the home cage for 25 min, an estimated time period for CNO to reach the target area and be effective, before being transferred to individual fresh cages (with estrous female urine added to the center of filter paper and rubbed onto the nose of the mice) to assay for micturition patterns for two hours (as described above).

To silence *Vgat*+ MPOA neurons, pair-housed *Slc32a1<sup>ires-Cre</sup>* male mice were injected with AAV-DIO-hM4Di-mCherry (AAV2/8-Elfα-DIO-hM4Di-mCherry) bilaterally in MPOA and underwent behavioral testing as described above.

### Immunohistochemistry and RNA In Situ Hybridization

Brains fixed in 4% paraformaldehyde were sectioned to 50 μm for immunohistochemistry. Primary antibodies used include rabbit anti-NeuN (1:1,000; ABN78, Millipore), rabbit anti-tyrosine-hydroxylase (1:2,000; AB152, Millipore) and rabbit anti-*c-fos* (1:1,000; Santa Cruz). Alexa Fluor 488-conjugated secondary antibodies against rabbit IgG (Invitrogen) were diluted 1:1,000. Fluorescent mRNA in situ hybridization was performed on 25 μm frozen sections and carried out with two methods: First, in situ hybridization of *Slc17a7*, *Slc17a6*, *Slc17a8*, *Gad1*, *Gad2*, *Crh*, *Cre*, and *RABVgp1* was performed using RNAscope assays according to the manufacturer's instructions (Advanced Cell Diagnostics). Second, antisense complementary RNA probes of *Crh* and *tdTomato* were labeled with digoxigenin (Roche), fluorescein (Roche), or dinitrophenol (PerkinElmer). Probes were detected with horseradish peroxidase-conjugated antibodies, amplified with biotin-conjugated tyramide and subsequently visualized with Alexa Fluor 488- or 568-conjugated streptavidin, or directly visualized with the TSA plus cyanine 3 system, as previously described (Wu et al., 2014). Image stacks were acquired with an Olympus FV1000 or a Leica SP8 laser scanning confocal microscope.

To determine the total number of cells (DAPI staining) and neurons (NeuN staining) in PMC, immunohistochemistry labeling was performed on 50 μm consecutive brainstem slices from *Crh<sup>ires-Cre</sup>::Rosa26<sup>lsI-tdTomato</sup>* mice. Z-stacks of each slice were acquired with an Olympus FV1000 confocal laser-scanning microscope with a 20X objective. After the boundary of PMC was manually outlined based on a gap in NeuN signal that surrounds the tdTomato labeled PMC, automatic cell counting was performed using ImageJ with custom-written macro scripts. Cell counts from consecutive PMC slices were accumulated to obtain the total PMC cell count.

### Rabies-Based Retrograde Trans-synaptic Tracing with Serial Two-Photon Tomography

TVA, a receptor of an avian virus envelope protein (EnvA), and rabies glycoprotein (RG) were introduced specifically in *Crh*+ PMC neurons through two Cre-dependent viruses (AAV-DIO-TVA-mCherry and AAV-DIO-RG, Miyamichi et al., 2013) injected intracranially. After three weeks of expression, RG-deleted (ΔRG) rabies virus encoding EGFP and pseudotyped with EnvA (RbV-EGFP) was injected intracranially. This combination of viruses limits the initial rabies infection largely to *Crh*+ neurons expressing TVA receptor, and labels “starter” neurons with both red (TVA-mCherry) and green (EGFP) fluorophores. RbV spreads *trans*-synaptically only from cells also expressing RG, thereby limiting monosynaptic tracing from neurons expressing both TVA and RG. These secondarily infected cells will express only EGFP encoded by RbV as they lack TVA-mCherry. In mice that received both helper viruses and RbV-EGFP expression, the brains were prepared for histology and analysis one week after RbV injection.

Animals were perfused transcardially with ice-cold phosphate buffered saline (PBS) followed by 4% paraformaldehyde (PFA) 7 days after RbV-EGFP infection. After an overnight fix in 4% PFA, brains were equilibrated in 30% sucrose solution for at least 48 hr. Whole brain samples were then sliced at 50 μm thickness using a freezing sliding microtome (Leica SM2010 R) and every other section was mounted on Superfrost Plus (Fisher Scientific) slides. Slides were coverslipped with Prolong Antifade mounting media containing DAPI (Molecular Probes) and imaged with an Olympus VS120 slide-scanning microscope using 10X objective. Putative presynaptic neurons expressing EGFP were manually assigned to specific brain regions based on Allen Brain Atlas, using landmarks visualized in DAPI and autofluorescence from the tissue.

For serial 2-photon (STP) tomography experiments, RbV-EGFP injected animals were perfused transcardially with ice-cold PBS followed by 4% PFA. After a 24 hr post-fix in 4% PFA, brains were kept in 0.7% glycine solution for 48 hr. The brainstem portion

containing PMC was blocked off, sliced at 50  $\mu\text{m}$  thickness using a freezing microtome, and imaged as described above to verify the infection of *Crh*+ PMC starter neurons. The anterior portion of the brain was stored in PBS before embedding in 4% agarose in 0.05 M PB, cross-linked in 0.2% sodium borohydrate solution, and imaged with a high-speed 2-photon microscope with integrated vibratome sectioning (x-y resolution of 1  $\mu\text{m}$ ; z-step of 50  $\mu\text{m}$ ; TissueCyte 1000, TissueVision) as described previously (Ragan et al., 2012). The raw image files were corrected for inhomogeneous illumination and light collection, stitched in 2D, and aligned in 3D. EGFP-positive neurons were automatically detected by a convolutional network trained to recognize cytoplasmic neuronal cell body labeling (Turaga et al., 2010), visually validated, reconstructed in 3D, and registered to a 3D reference brain based on the Allen Brain Atlas (Kim et al., 2015; Sunkin et al., 2013) by affine followed by B-spline transformation using the software Elastix (Klein et al., 2010). The number of total input neurons in each brain region was normalized by the total number of RbV-EGFP positive neurons in the belonging macro structure (e.g., cortex) to account for the variability in the total number of labeled candidate input neurons.

### QUANTIFICATION AND STATISTICAL ANALYSIS

Behavioral sample sizes were chosen based on common practice in animal behavior experiments. Statistical parameters including the value of *n*, measurements of arithmetic mean and standard error of the mean (mean  $\pm$  SEM), statistical tests and significance are reported in the Figures and the Figure Legends. In figures, asterisks denote statistical significance as calculated by the specified statistical tests (\*,  $p < 0.05$ ; \*\*,  $p < 0.01$ ; \*\*\*,  $p < 0.001$ , ns, not significant). Details in quantification and analysis for behavior, anatomy, electrophysiology, cystometry, and fiber photometry data are described in the corresponding sections.

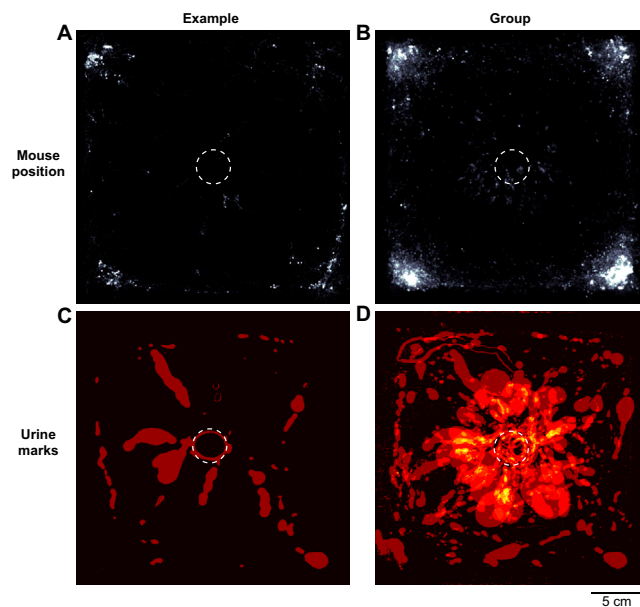


**Figure S1. Distinct Spatial Distributions of Mouse Position and Urine Marks, Related to Figure 1**

(A and B) Real-time tracking of mouse center position in an open-field arena (26 cm X 26 cm) with estrous female urine stimulus added to the center (dotted circle) reveals that mice spend a majority of the time at the corners of the cage, and a small fraction of the time near the center stimulus. (A), Single mouse in a 10 min trial (Example), (B), Overlay of group data ( $n = 6$  mice, 4 trials each). Lighter color pixels indicate more time spent at the position.

(C and D) In contrast to mouse position, the majority of urine marks are deposited near the center stimulus in example (C) and overlay of group (D) data. Lighter color pixels in the group data indicate more overlap of urine marks from different trials. Female urine stimulus added to the center of arena is removed from the image and does not count toward the overlap.

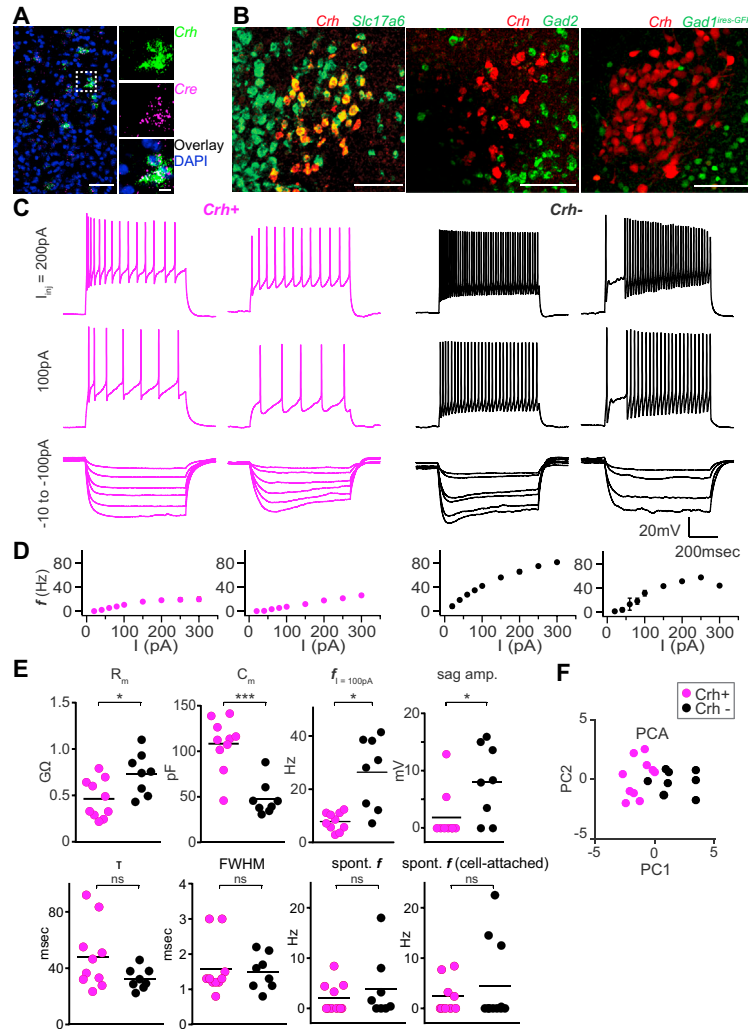


**Figure S2. Cellular Composition and Electrophysiological Properties of PMC, Related to Figure 2**

(A) Co-labeling of *Crh* (green) and *Cre* (magenta) in *Crh<sup>iRes-Cre</sup>* mice by mRNA in situ hybridization indicates near perfect overlap in PMC. Scale bar: 50  $\mu\text{m}$ , (inset) 25  $\mu\text{m}$ .

(B) *left*, Co-labeling of *Crh* and *tdTomato* in *Slc17a6<sup>iRes-Cre</sup>::Rosa26<sup>sls</sup>-tdTomato* mice by mRNA in situ hybridization indicates near perfect overlap in PMC; *center*, Co-labeling of *Crh* and *tdTomato* in *Gad2<sup>iRes-Cre</sup>::Rosa26<sup>sls</sup>-tdTomato* mice by mRNA in situ hybridization indicates little overlap between *Crh* and *Gad2*, and that some *Crh*-negative cells are *Gad2*-positive in PMC; *right*, *Crh<sup>iRes-Cre</sup>::Rosa26<sup>sls</sup>-tdTomato::Gad1<sup>iRes-GFP</sup>* indicates no overlap between *Crh* and *Gad1* in PMC. Scale bar: 100  $\mu\text{m}$ .

(C) Example current-clamp recordings from two *Crh+* (*left*, magenta) and two *Crh-* (*right*, black) neurons in an acute brain slice containing PMC showing heterogeneous responses to current injections.

(D) Average firing rates ( $f$ ) as functions of the current step amplitude ( $I$ ) for each of the neurons shown in (A). Error bars depict SEM across trials ( $n = 3-4$ ) but are often smaller than the symbol size.

(E) Summary of cellular and electrophysiological parameters that factored into principal component analysis (Figure S2F). Top: Membrane resistance ( $R_m$ ), membrane capacitance ( $C_m$ ), firing rate with 100 pA current injection ( $f_{I=100\text{pA}}$ ), and amplitude of sag current ( $I_h$ , sag amp.) distributions distinguish between *Crh+* and *Crh-* neurons in PMC; bottom, time constant ( $\tau$ ), action potential width (full width at half maximum, FWHM), spontaneous firing rates measured in whole-cell configuration with  $\text{K}^+$ -based internal solution without current injection (spont.  $f$ ), as well as in cell-attached configuration with artificial cerebral spinal fluid (ACSF) in the recording pipette (cell-attached). Black bars, mean. ns: not significant, \* $p < 0.05$ , \*\* $p < 0.005$ , \*\*\* $p < 0.0005$ , two-tailed Mann-Whitney U test.

(F) PCA shows separation between *Crh+* and *Crh-* neurons, where the first principal component is primarily comprised of  $C_m$  and  $f_{I=100\text{pA}}$ .

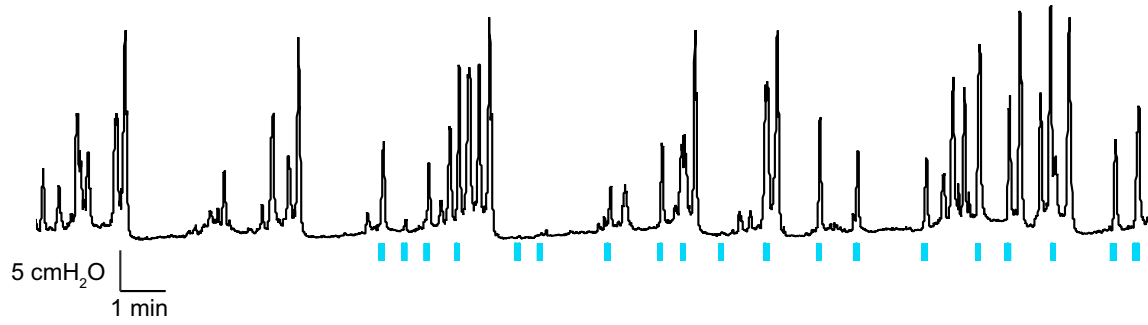


**Figure S3. Optogenetic Activation of Crh+ PMC Neurons in the PMC with Randomized Light Interval, Related to Figure 3**

Example bladder pressure trace from a mouse expressing ChR2-tdTomato in PMC *Crh*+ neurons with 473nm light delivered at randomized intervals between 30 s and 90 s.

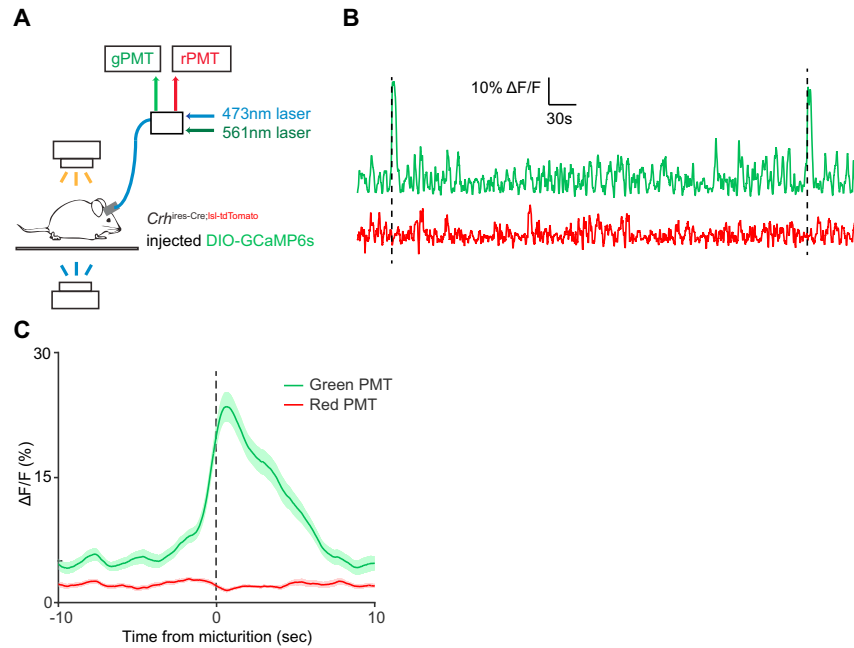


**Figure S4. Simultaneous Recording of Micturition Events and Two-Color Fiber Photometry, Related to Figure 4**

(A) Setup of 2-color fiber photometry with the addition of a reference red channel in *Crh<sup>ires-Cre::Rosa26<sup>Isl1</sup>tdTomato</sup>* animals injected with Cre-dependent GCaMP6s.

(B) Example 2-color fiber photometry traces, overlaid with black dotted bars indicating two micturition initiation bouts.

(C) Averaged fiber photometry signals aligned to the initiation of each micturition event at  $t = 0$  ( $n = 2$  mice, 48 micturition events). Simultaneous recordings showed that intensity of GCaMP6s fluorescence, but not tdTomato, positively correlated with awake urine release. Shaded area represents SEM.

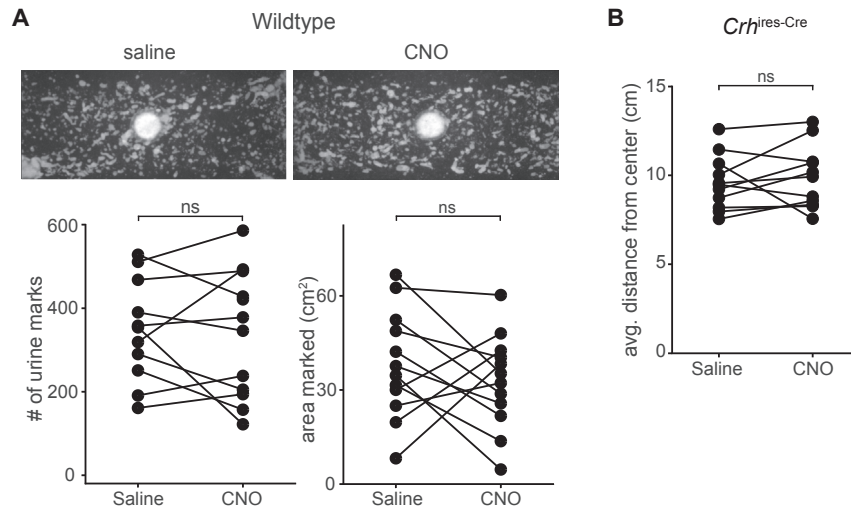


**Figure S5. Control Experiments for CNO Effect on Micturition, Related to Figure 5**

(A) *top*, Example micturition pattern from a wild-type mouse with saline or CNO IP injection; *bottom*, number of urine marks deposited (left) and total area on the filter paper marked by urine (right) were not changed in CNO trials compared to saline trials. ns: not significant, Wilcoxon matched-pairs signed rank test.

(B) Spatial distribution of remaining urine marks in CNO-treated *CrtHires-Cre* mice, as indicated by their average distance from stimulus center, is unaffected compared to saline trials. ns: not significant, Wilcoxon matched-pairs signed rank test.

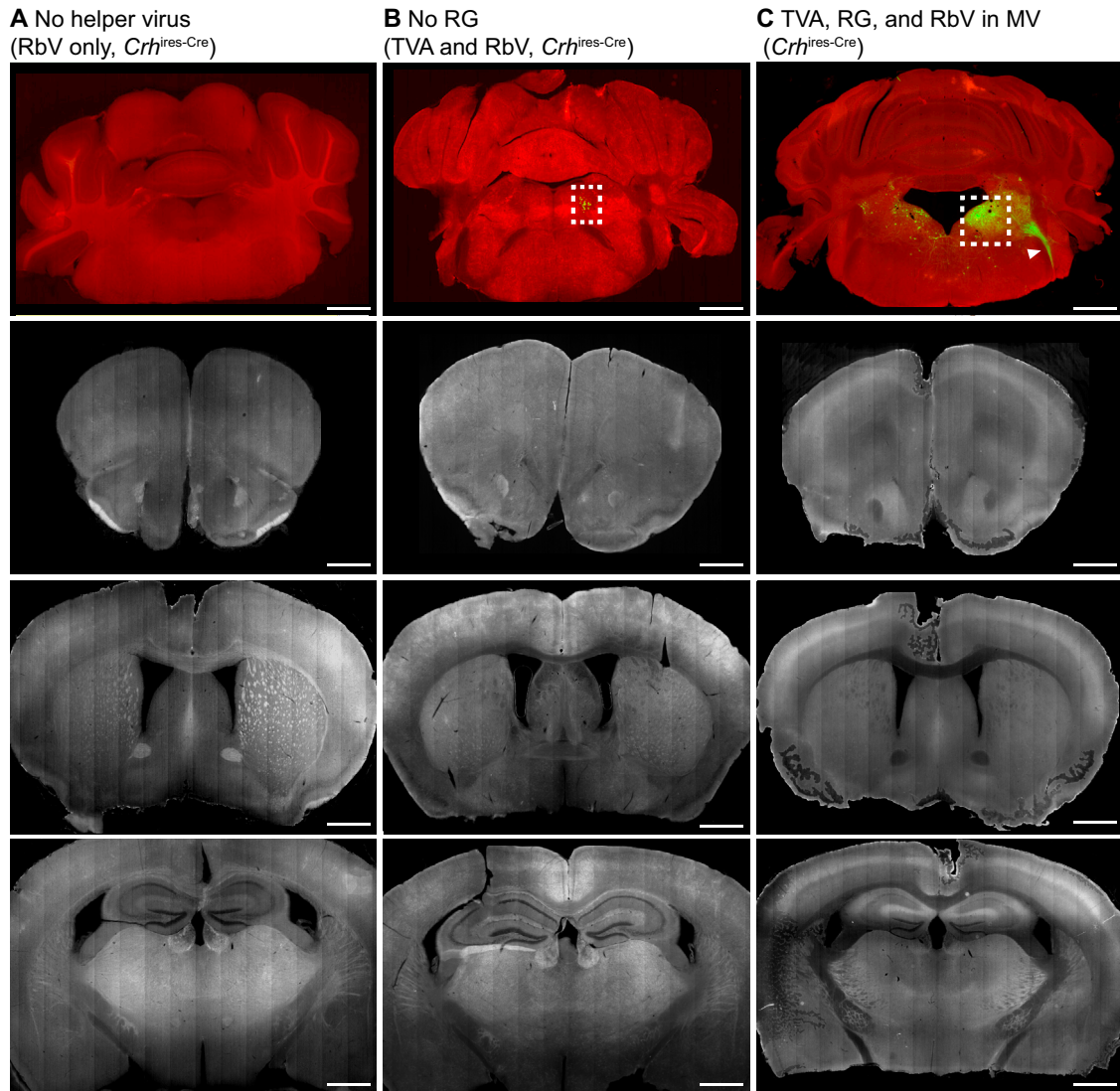


**Figure S6. Control Experiments for Rabies Tracing, Related to Figure 6**

(A) Helper virus injection was omitted, and RbV-EGFP was injected into a *Crh*<sup>ires-Cre</sup> mouse. No EGFP+ cells were observed in or around the PMc (upper panel). No long-range EGFP+ input cells were present elsewhere in the brain (lower panels, three representative sections). Scale bars: 1 mm.

(B) AAV-DIO-RG was omitted from the helper AAV injection into a *Crh*<sup>ires-Cre</sup> mouse, and RbV-EGFP was subsequently injected. Starter cell infection was observed in PMc (dashed line, upper panel), but no long-range EGFP+ cells were observed elsewhere in the brain (lower panels). Scale bars: 1 mm.

(C) Helper AAVs (AAV-DIO-TVA-mCherry and AAV-DIO-RG) and RbV-EGFP were targeted into the Medial Vestibular nucleus (MV) of a *Crh*<sup>ires-Cre</sup> mouse. Robust starter cell infection was observed in MV (dashed line), and 8<sup>th</sup> cranial nerve (arrowhead) was also labeled with RbV-EGFP (upper panel). However, very few long-range EGFP+ cells were present elsewhere in the brain (lower panels). Scale bars: 1 mm.

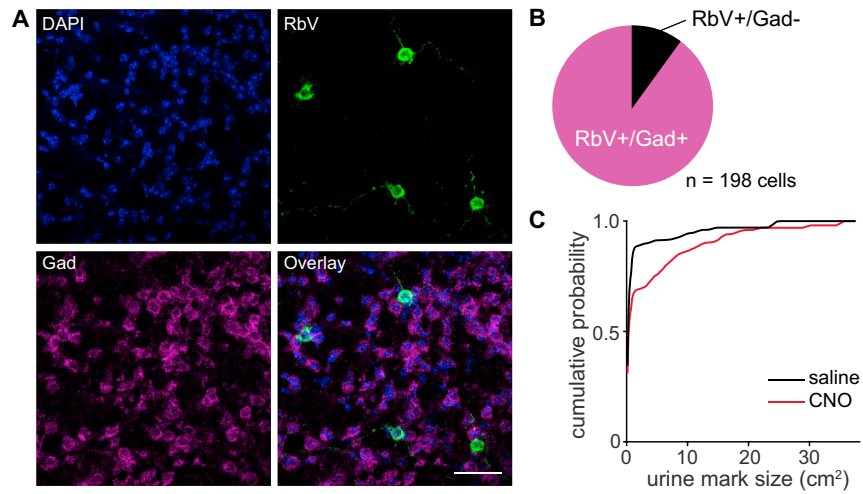


**Figure S7. Cell Type of Rabies-Labeled MPOA Neurons and Effect of Neuronal Inhibition on Urine Mark Size, Related to Figure 7**

(A) In situ hybridization of Gad (*Gad1* and *Gad2*, magenta) and rabies virus (RbV) nucleoprotein (green) mRNAs reveals that a majority of cells in MPOA retrogradely labeled from *Crh*+ PMC cells express GABA synthetic enzymes. Scale bar: 50  $\mu$ m.

(B) Quantification of cell type of retrogradely labeled cells in MPOA.

(C) Cumulative distribution of size of urine marks shows different spot sizes in CNO (red) and saline (black) trials.